Available online at www.sciencedirect.com
ScienceDirect
Tectonophysics 445 (2007) 3–25
TECTONOPHYSICS
www.elsevier.com/locate/tecto

Deep array electromagnetic sounding on the Baltic Shield: External excitation model and implications for upper mantle conductivity studies

Elena Yu. Sokolova *, Ivan M. Varentsov
BEAR Working Group

Geoelectromagnetic Research Centre, Inst. of Physics of the Earth, Russian Academy of Sciences, 142190, POB 30, Troitsk, Moscow Region, Russia

Received 1 December 2005; accepted 25 June 2007
Available online 31 July 2007

Abstract

The BEAR array of simultaneous electromagnetic (EM) observations probes the deep crustal and upper mantle conductivity structure of the Baltic Shield searching for the lithosphere–asthenosphere boundary beneath. The adequate interpretation of the results of this unique high latitude natural field EM sounding requires proper understanding of the actual external excitation conditions because conventionally used plane wave model assumptions may be substantially violated in the vicinity of inhomogeneous polar sources. The paper presents an overview of the morphology and statistics of source distortions in the BEAR EM field transfer functions (TF) and the ways of their suppression. The stability of the final TF estimates obtained with the exclusion of intensive non-stationary auroral effects is further justified. The external excitation model effective for the whole BEAR observation period is inferred from the array distribution of the inter-station geomagnetic transfer functions. The model is supported by the results of polar ionosphere–magnetosphere current system studies, based on the simultaneous ground and satellite geomagnetic observations, and sets bounds for the "plane wave" approach in the BEAR data interpretation to avoid unfounded inferences on the upper mantle electrical properties. The signatures of the lithosphere–asthenospere boundary under Fennoscandia derived from the BEAR data are summarized and its resolution within the traditional plane wave interpretational paradigm is analysed assuming the presented external source pattern and estimated TF uncertainties caused by the source inhomogeneity.

Keywords: Natural electromagnetic fields; Array soundings; Inhomogeneous excitation; Transfer functions; Electrical conductivity; Lithosphere; Asthenosphere

1. Introduction

The Baltic Electromagnetic Array Research (BEAR) held in June–July, 1998 is the largest-scale natural EM field sounding experiment at high latitudes probing the deep crustal and upper mantle geoelectrical structure of the Baltic (Fennoscandian) Shield (BEAR WG, 1999; Korja et al., 2002). This research continues long lasting investigations of the electrical conductivity of the lithosphere of Fennoscandia, resulted in a number of previous publications (Kaikkonen et al., 1983; Jones et al., 1983; Pajunpaa, 1987; Rasmussen et al., 1987; Kovtun, 1989; Korja and Hjelt, 1993; Korja and Koivukoski, 1994). The BEAR project is focused on the main goal to establish the geoelectric signatures of a lithoshpere–asthenosphere

* Corresponding author. Tel./fax: +7 495 7777218.
E-mail address: igemi3@mail.transit.ru (E. Yu. Sokolova).

0040-1951/$ - see front matter © 2007 Published by Elsevier B.V.
doi:10.1016/j.tecto.2007.07.006

boundary under the ancient shield basing on the extended settings of the sounding array, long term simultaneous observations and modern advances in the data acquisition, analysis and interpretation techniques.

On the way to this target the project encounters two principal obstacles. The first one, connected with the necessity of probing the deep electrical conductivity structure in the presence of highly heterogeneous crust of the Shield, was treated in special studies integrating all the information from the previous EM soundings in Fennoscandia (Korja et al., 2002; Engels et al., 2002; Varentsov et al., 2002). These studies resulted in the construction of the generalized geoelectric crustal thin-sheet (SMAP) and volume (VMAP) models and the deep normal section till mid-mantle depth for Fennoscandia as a background for the investigation of upper mantle anomalies and brought a variety of simulated EM responses useful for the BEAR data interpretation. The recent paper of Lahti et al. (2005) concentrates on the invariant analysis of the BEAR magnetotelluric responses and yields the principal understanding of the character of distortions caused by the inhomogeneous upper crust.

The present paper addresses another challenging problem of the BEAR data ensemble originated from the high latitude location of the array, which involves 46 five-component magnetotelluric (MT) sites approaching the Polar circle and 20 geomagnetic deep soundings (GDS), going as far as 79°N (Fig. 1). The transfer functions (TF), connecting different observed EM field components in frequency domain, can be directly interpreted in the terms of Earth's electrical conductivity only under certain assumption on the EM field excitation (Weidelt, 1978; Dmitriev and Berdichevsky, 1979): they lose their source invariance in the presence of substantial external field inhomogeneities. The proximity of the complex sub-polar ionospheric sources to the BEAR array requires a special attention to their distorting influence, which may lead to erroneous interpretation of the sounding results. The TF estimation for these array observations made with a number of advanced robust procedures (Egbert, 1997; Smirnov, 2003; Varentsov et al., 2003a) yields a prominent stability of results independently estimated for the sequence of records during the observation period. The primary understanding of the source phenomena for the BEAR sounding was given by Engels et al. (2002) and Vanyan et al. (2002a) and was extended in many details by Varentsov et al. (2003b). The latter paper, in particular, explains the effectiveness of the applied data processing tools for the elimination of the variety of events with inhomogeneous external field.

We start the paper with new illustrations of the temporal stability of TF responses at selected array sites, and then concentrate on the clarification of the actual external excitation conditions for the BEAR sounding. Further on, we introduce an effective model of the external geomagnetic field for the whole duration of the BEAR experiment, inferred from the inter-station geomagnetic transfer functions and supported by the study of ionosphere–magnetosphere current systems, based on the complex of ground and satellite geomagnetic data. This model gives serious grounds to discuss the limits of traditional magnetotelluric MT and GDS interpretation approaches for the BEAR TF ensemble. We consequently examine the scale of remaining source influence in different TF data components and give recommendations/restrictions on their usage in the geoelectrical studies to prevent erroneous interpretation.

The investigation of MT/GDS sounding excitation problems, which are in the focus of the paper, help to elaborate the adequate methodology of long-period data analysis and have many issues concerning the study of the deep geoelectric structure. In particular, it gives new clear arguments for the discussion on the Fennoscandian upper mantle electrical anisotropy (Bahr and Simpson, 2002; Varentsov et al., 2002; Lahti et al., 2005). Finally, we describe the first assumptions on the regional lithosphere–asthenosphere structure inferred from the BEAR observations and discuss their reliability, taking into account the data validity factors, the resolution bounds, derived from the modelling studies (Engels et al., 2002; Varentsov et al., 2002), and the estimates of source distortion scale in the resulting transfer functions.

2. Detection and elimination of non-stationary source effects in the BEAR transfer functions

The natural EM field excitation at high latitudes is performed mostly by ionospheric and magnetospheric current systems located in the polar cap and sub-polar areas, producing non-uniform primary field with specific temporal events being quite far from the plane wave approximation. The most severe disturbing agent is a polar electrojet representing a quasi-linear current system variable in time and space. It is studied in connection with EM soundings in a number of papers (Hermance, 1978; Mareschal, 1986; Osipova et al., 1989), which presented its simplified static and first dynamic models and estimates of related TF distortions. The recent studies of Viljanen et al. (1999), Engels et al. (2002), Vanyan et al. (2002a,b) suggest more realistic models of polar source geometry and outline variability of TF distortions dependent on inhomogeneities in both the source and the Earth's conductivity structure. In particular, the advanced study of Engels et al. (2002), based on the

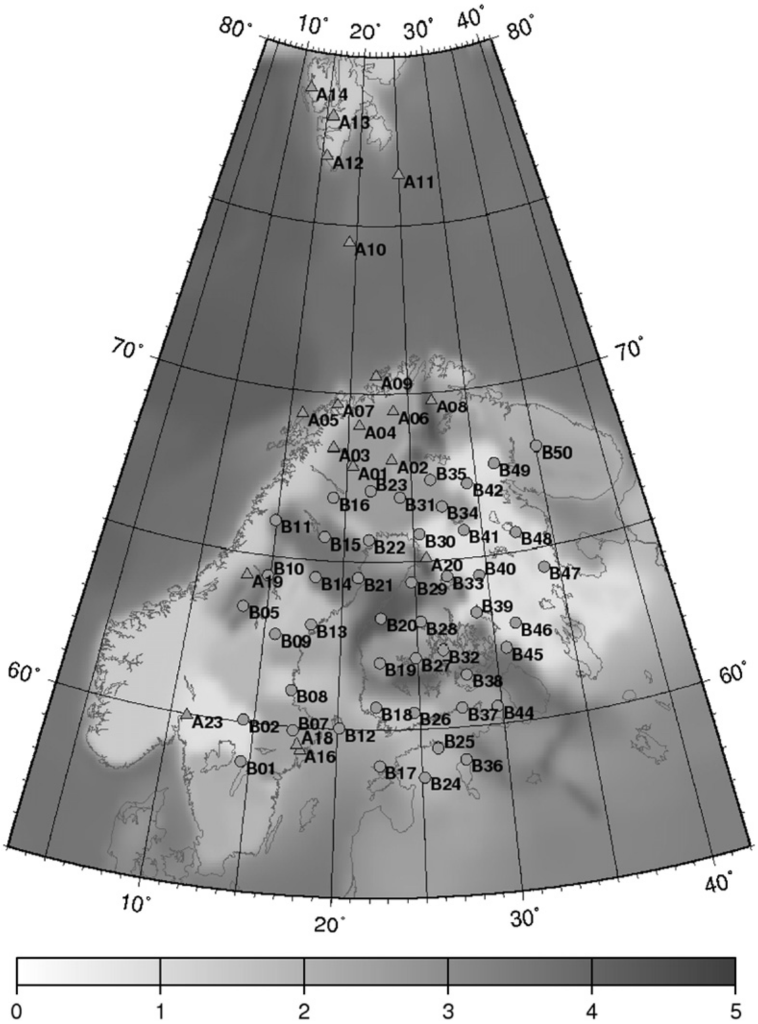

Fig. 1. The BEAR array of simultaneous five-component MT sounding sites (circles) and GDS observations (triangles), depicted on a priori conductance map of the upper 60 km lithosphere layer (Korja et al., 2002); the gray palette gives the decimal logarithm of conductance (in S).

detailed a priori multisheet geoelectric model of Fennoscandia (Korja et al., 2002), jointly examined the influence of 3D crustal heterogeneity and 3D source geometry on the long period TF responses related to the upper mantle targets. The realistic approximation of the polar electrojet was constructed in the form of equivalent system of horizontal elementary dipoles at the ionospheric height. This approach outlined a complicated mosaic spatial pattern of source distortions over the Baltic Shield, changing with period and reflecting the coupling effects of crustal conductivity variations and EM sources inhomogeneities. These distortions, in spite of the static source approximation, have much smaller amplitudes than in traditional dipole and line source models over the layered Earth. The available studies with the elements of dynamic source approximation (Hermance, 1978; Vanyan et al., 2002a) demonstrate further smoothing and diminishing of distorting effects for the moving inhomogeneous source in comparison with static representation. Therefore, we have a number of indications how the temporal and spatial interference of strictly inhomogeneous source events extends the spatial wavelength of the “effective” source in the approach to the plane wave pattern. However, the existing numerical source models are still far from the sufficient joint account of spatial and temporal details and cannot yield the quantitative measure of the temporal averaging effects in TF estimation within a long time window as well as of averaging effects for numerous sources acting simultaneously.

The major impact for the understanding of the source distortion scale in each particular EM sounding, with its specific pattern of the external field temporal and spatial behaviour, still comes directly from the data acquired. The recent EM experiments at high latitudes, namely GDS soundings in Greenland (Engels, 1997) and MT studies in Polar Canada (Garcia et al., 1997; Jones and Spratt, 2002), equipped with a new generation of robust data processing techniques, demonstrated a success in suppression of source distortions. The current study presents the broad experience with the treatment of the source problem for the simultaneous observations of the BEAR array in Fennoscandia during the summer of 1998.

The full set of the MT and GDS responses for the BEAR array consists of impedance **Z** and tipper $\mathbf{W_Z}$ local estimates at a local site **r**:

$$\begin{pmatrix} E_x^r \\ E_y^r \end{pmatrix} = \mathbf{Z}\begin{pmatrix} H_x^r \\ H_y^r \end{pmatrix} = \begin{pmatrix} Z_{xx} & Z_{xy} \\ Z_{yx} & Z_{yy} \end{pmatrix}\begin{pmatrix} H_x^r \\ H_y^r \end{pmatrix},$$

$$H_2^r = \mathbf{W_Z}\begin{pmatrix} H_x^r \\ H_y^r \end{pmatrix} = \begin{pmatrix} W_{zx} & W_{zy} \end{pmatrix}\begin{pmatrix} H_x^r \\ H_y^r \end{pmatrix};$$

and inter-station operators of horizontal magnetic tensor **M** and regional tipper $\mathbf{S_z}$, defined for a pair of sites, local **r** and base $\mathbf{r}^0$:

$$\begin{pmatrix} H_x^r \\ H_y^r \end{pmatrix} = \mathbf{M}\begin{pmatrix} H_x^{r^0} \\ H_y^{r^0} \end{pmatrix} = \begin{pmatrix} M_{xx} & M_{xy} \\ M_{yx} & M_{yy} \end{pmatrix}\begin{pmatrix} H_x^{r^0} \\ H_y^{r^0} \end{pmatrix},$$

$$H_2^r = \mathbf{S_z}\begin{pmatrix} H_x^{r^0} \\ H_y^{r^0} \end{pmatrix} = \begin{pmatrix} S_{zx} & S_{zy} \end{pmatrix}\begin{pmatrix} H_x^{r^0} \\ H_y^{r^0} \end{pmatrix}.$$

The local TF data were estimated independently by three BEAR project teams with different robust remote reference (RR) processing techniques (Egbert, 1997; Smirnov, 2003; Varentsov et al., 2003a) and finally subjected to a multi-team robust averaging (Varentsov et al., 2003a). The resulting data show no visible polar source distortions at almost all sites until a period of 3 h, and demonstrate in this range a prominent temporal stability for 10–14 day-long separate records. An evident source influence was encountered only in long period tipper responses at 3–24 h. Fig. 2 outlines these stability and instability features of the impedance and tipper at quite typical BEAR sites B41 (Finnish Karelia) and B15 (Northern Sweden). The single-site estimates for single data records are presented here because they should demonstrate greater source distortions comparing with the final multi-record multi-RR averaged responses. The impedance curves for separate records are almost coincident for all amplitude and phase components up to 3-hour period. For longer periods their temporal scatter is quite random. The spatial variability (from site to site) of this scatter also looks random.

The corresponding comparison of the tipper data shows larger variability, which is connected primarily with the general weakness of the vertical geomagnetic field relative to the horizontal one and with the small $\mathbf{W_z}$ amplitudes observed at many BEAR sites. Note, that sites with large tipper values, caused by geoelectric anomalies (like B15 in Fig. 2), are characterized by higher stability of $\mathbf{W_z}$ estimation and better fit of the estimates for separate records. At short periods (tens of seconds) tippers have local noise bias more pronounced then impedances, however, these bias effects are effectively eliminated at the following multi-RR processing stage (Varentsov et al., 2003a). The temporal scatter of tipper components at the periods of 2–3 h increases but still stays random from record to record permitting effective averaging of the whole set of estimates. However for periods greater then 3 h, in contrast to impedance, we see a strong upward bias of tipper amplitudes, caused by external source geometry. In this range at most of the BEAR sites the external (source influenced) tipper part prevails over the internal (geoelectric) contribution. More details of the long period tipper behaviour are discussed in the following section. The similar analysis of temporal variability of the horizontal magnetic tensor estimates for the base site B22 (Fig. 1) (Varentsov et al., 2003b) revealed almost the same stability level in the broad period range from 15 s to 12–24 h as for the impedance.

To trace the way to such stable results within our data processing procedure we applied the temporal monitoring approach at a more detailed level of partial TF estimates (obtained for a set of primary record extents involved into the spectral analysis) in connection with parameters of the source activity and inhomogeneity at the same temporal scale. This analysis outlines the fine-scale morphology and statistics of inhomogeneous excitation effects in TF estimates (Varentsov et al., 2003b). Fig. 3 illustrates the monitoring results at the site B11, located just at the Polar circle and being the northernmost BEAR site in geomagnetic coordinates. The time-period plots (pseudo sections) of partial estimates of the most disturbed **Z** and $\mathbf{W_z}$ components for a set of 11-hour sequential non-overlapping time windows within two first data records (54 extents, 25 days in total) show a number of significant outliers in the wide period range. These outliers are well seen on the background of the final multi-RR results, presented in three right- and leftmost columns. Fig. 4 shows the monitoring results for the same time window and TF data components, obtained for all four data records at B11 (92 extents in total), as graphs of period-averaged values of the partial horizontal magnetic field (input) coherence $\mathrm{Coh}^2(\mathbf{H_h})$, mutual coherence $\mathrm{Coh}^2(\mathbf{Z_y})$ for the pair of Z_{yx}, Z_{yy} components, $\mathbf{Z_y}=(Z_{yx}, Z_{yy})$ and mutual tipper coherence $\mathrm{Coh}^2(\mathbf{W_z})$. We also present here standard variation graphs for magnetic fields. This figure traces the

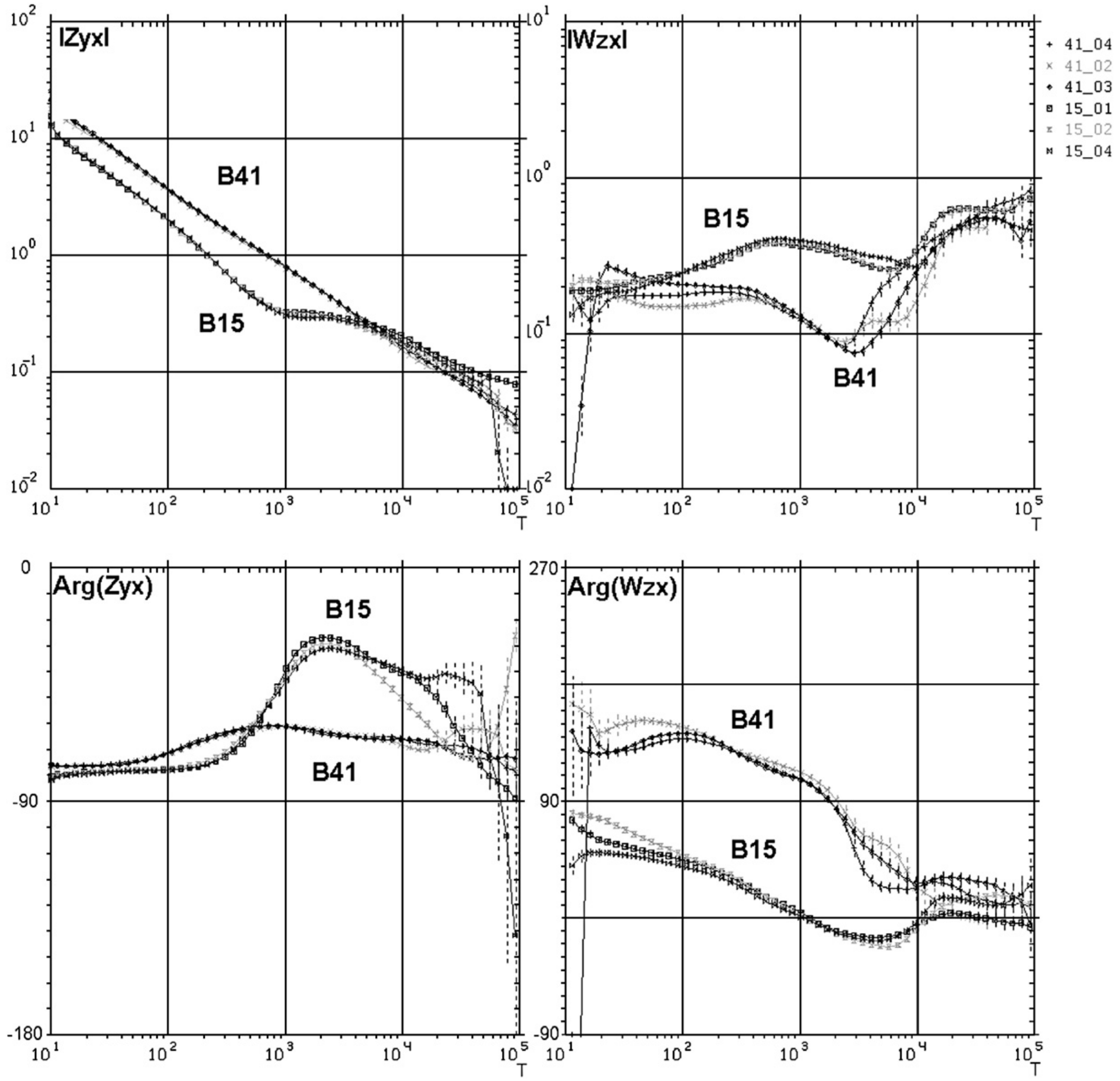

Fig. 2. The temporal stability of the BEAR estimates at sites B41 and B15 obtained independently for 3 data records 10–14 days-long; two left panels show Z_{yx} impedance components (top — amplitudes in mV/km/nT, bottom — phases in degrees); two right panels present W_{zx} tipper components (top — amplitudes, bottom — phases in degrees); site and record numbers are indicated in the legend; the horizontal logarithmic axes give the period (s).

sustainable correlation of the peaks in the geomagnetic field intensity with low mutual and high input period-averaged coherence at specific data extents. Figs. 3, 4 complement each other in demonstration of the principle fact, that most of extents with significant TF outliers are marked by (i) relatively high geomagnetic activity, (ii) the decreased quality of the considered linear relations and (iii) the increase of the horizontal magnetic field partial coherence.

The morphology of the impedance amplitude and phase curve distortions, caused by typical intensive sub-storms in the area below electrojets is shown in Fig. 5 for the same B11 site. The response “STORMS” corresponds to the average of partial estimates over the six 11-hour extents, containing the most severe polar sub-storms during the monitoring time. In comparison with the results of the robust stacking of “coherency sorted” data (Coh_S) they demonstrate the bias, which for amplitude is as much as 60% at the period of 6500 s and for phase reaches 15° at the period of 2500 s.

This monitoring procedure was applied at several other BEAR sites, and the following general conclusions has

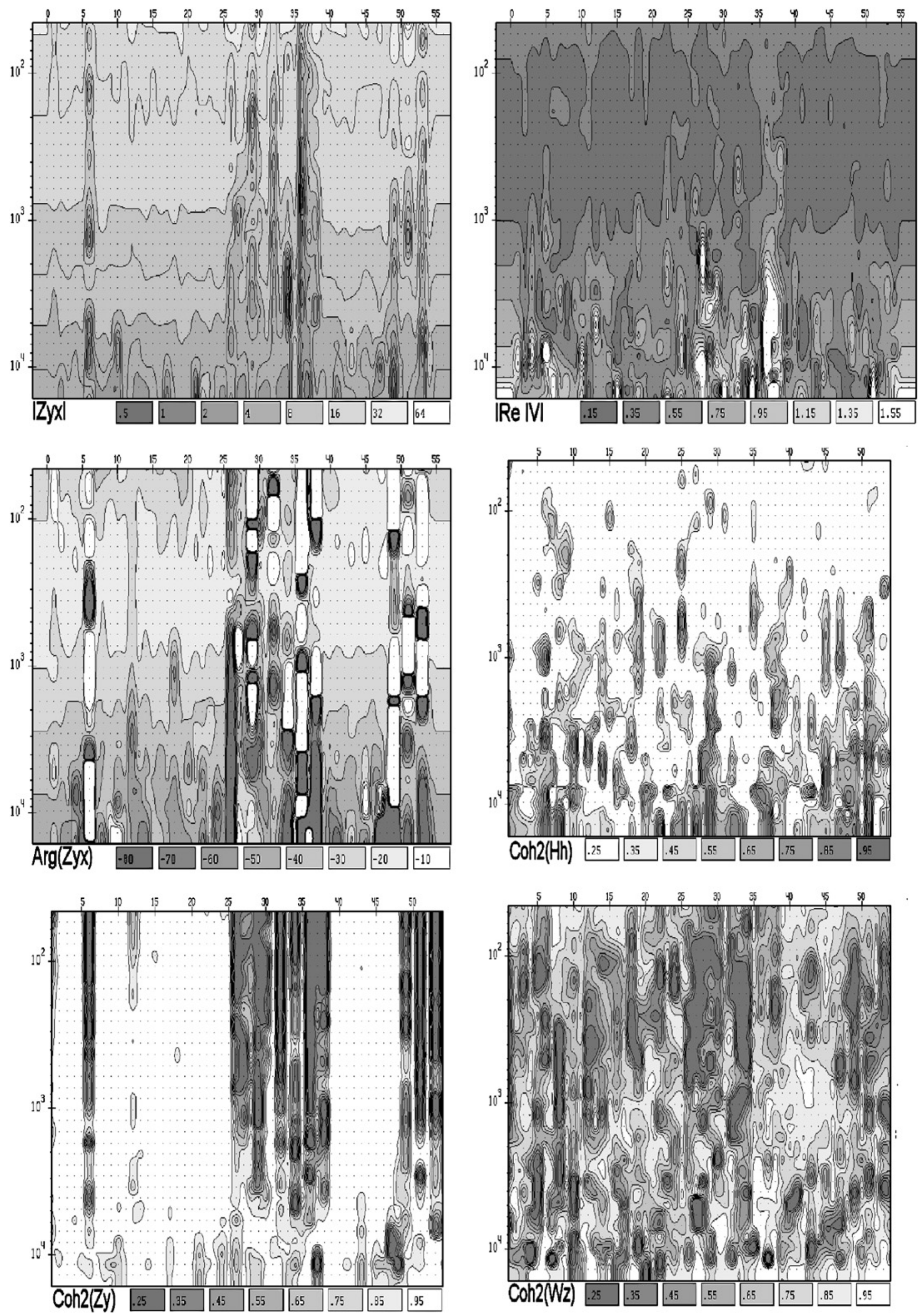

Fig. 3. Temporal variability sections of the impedance and tipper single-site partial estimates for the 11-hour window (site B11, first two records 25 days-long), left panels from top to bottom: impedance amplitudes, $|Z_{yx}|$, phases, $\mathrm{Arg}(Z_{yx})$ and related square multiple coherence, $\mathrm{Coh}^2(Z_y)$; right panels from top to bottom: real induction vector amplitudes, |Re IV|, and related square coherences, input horizontal magnetic, $\mathrm{Coh}^2(H_h)$, and multiple, $\mathrm{Coh}^2(W_z)$; the horizontal axis gives the numbers (1–54) of continuous non-overlapping 11-hour long record extents, the vertical logarithmic axis gives period (s); three leftmost and rightmost columns at TF panels additionally present correspondent final responses obtained by the robust stacking procedure.

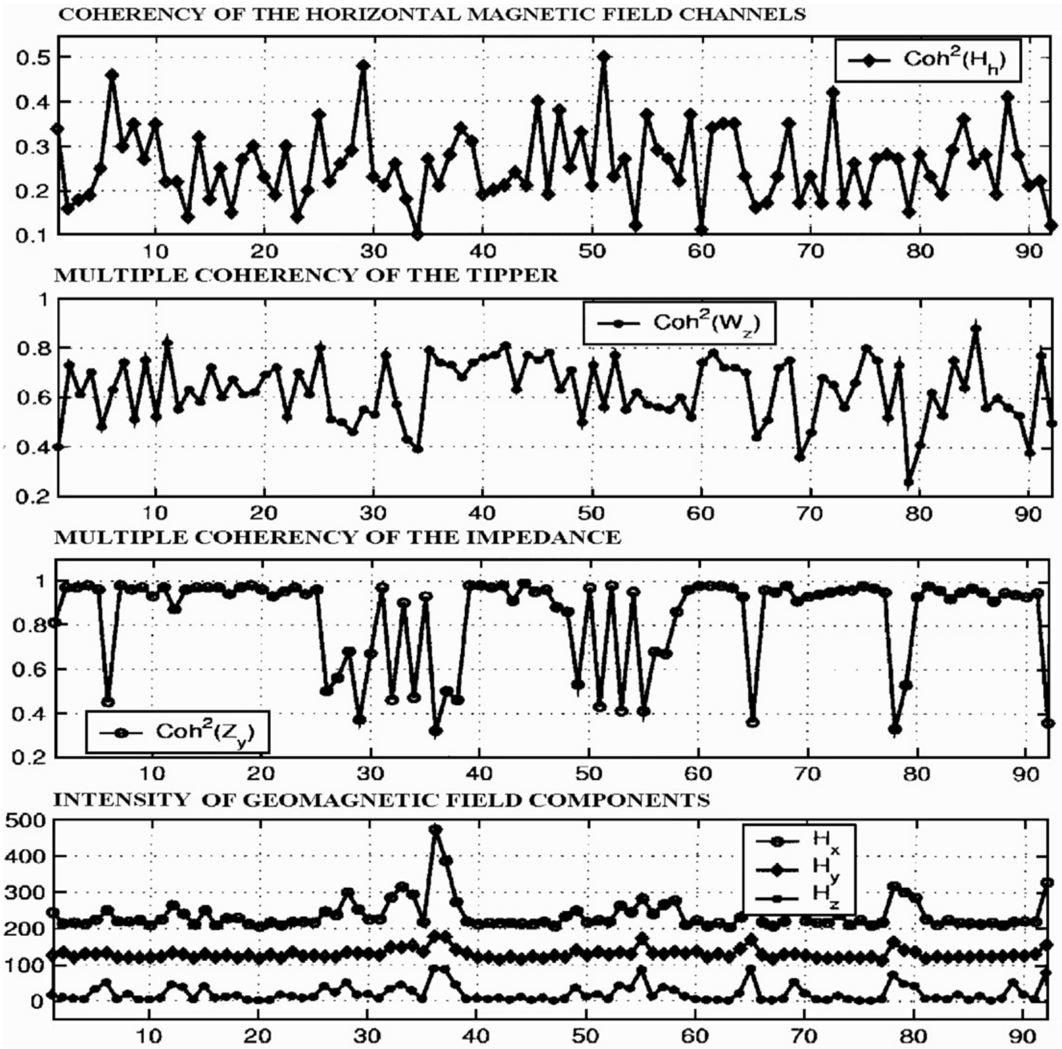

Fig. 4. The temporal variability of the period-averaged square coherence of partial TF estimates for the whole observation period at site B11: horizontal magnetic $\mathrm{Coh}^2(H_h)$, mutual impedance $\mathrm{Coh}^2(Z_y)$ and tipper $\mathrm{Coh}^2(W_z)$, compared with the variation intensity of magnetic components H_x, H_y, H_z; the horizontal axis gives numbers of continuous non-overlapping 11-hour long record extents (1–92) used to calculate coherence and intensity estimates.

been finally formulated: (i) windows with strongly distorted **Z**, $\mathbf{W_z}$ and **M** partial estimates correspond to the intensive inhomogeneous electrojet events; (ii) these distortions form strong outliers at the sides of quasi-normal distributions of partial estimates; (iii) there is a good correlation between source TF distortions and the anomalies of corresponding coherence estimates, namely, the increased input coherence for the dominant harmonics of sub-storms (1–3 h) with quasi-linear polarization, and the decreased mutual coherence at relatively shorter periods (the most pronounced in the impedance data).

These conclusions approve the importance of event rejection criteria, based on the averaged mutual/input coherence, which were applied in the robust processing procedure (Varentsov et al., 2003a) and helped to eliminate significantly source effects even in the simplest single-record single-site estimates (Fig. 2). Fig. 5 illustrates the effectiveness of this technique comparing the trivial estimates (No_Coh_S), obtained without application of the coherence-based sorting of the partial estimates stacked for all data records at site B11, with the coherence-sorted robust average (Coh_S), which provides the profound improvement of results. The downward amplitude bias (up to 30% at the periods greater then 2500 s) and the phase shift (up to 10°) in the No_Coh_S estimate are similar in morphology with typical distortions,

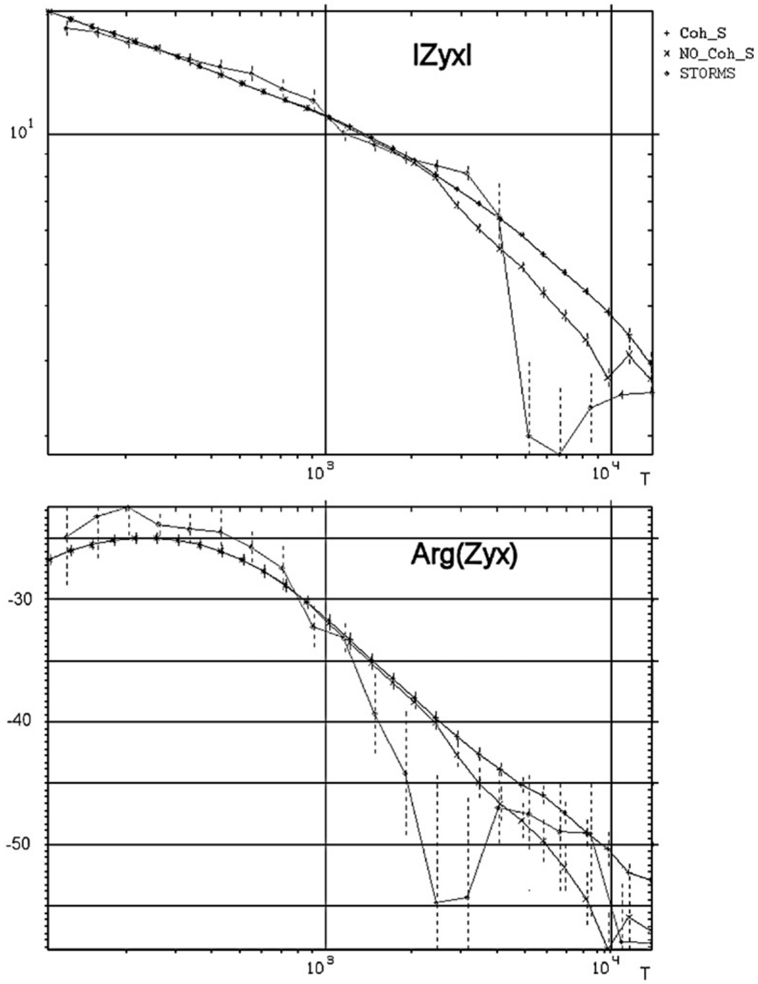

Fig. 5. The comparison of Z_{yx} amplitude (top, in mV/km/nT) and phase (bottom, in degrees) responses at B11 site obtained as a result of the robust stacking of partial estimates for 11-hour long record extents (1–92) with (Coh_S) and without (NO_Coh_S) coherency-based sorting together with an extreme average estimate (STORMS) for six 11-hour long extents with the most severe sub-storm events during the BEAR experiment.

demonstrated by Osipova et al. (1989) for the static electrojet model. These disturbances may serve as an upper bound of the source distortions, that would be accumulated in the final TF estimates, obtained without special data sorting.

Within the conventional BEAR processing graph, on the way from the variability of partial estimates to the stability of the final stacked responses, the coherence-based sorting was followed by the use of multi-record and multi-RR robust estimators, which finally resulted in the profound reduction of different noise factors, including the source distortions (Varentsov et al., 2003a,b). Thus, the application of the adaptive robust processing schemes for prolonged BEAR observations in the conditions of the moderate geomagnetic activity in summer 1998 has brought the reliable elimination of the disturbing non-stationary effects caused by polar sub-storms. However, the source bias effects at a temporal scale longer than the 2-month duration of the BEAR experiment (and stationary in this sense) requires further examination.

3. Examination of stationary source effects in the final TF estimates

To examine the presence of “stationary” source-caused bias, which might remain in the resulting transfer functions as a cumulative influence of inhomogeneous external sources acting during the whole BEAR observation period, we searched for indicators of large-scale systematic distortions in the spatial TF images. The 3D modelling results obtained as a response on a plane-wave excitation in the generalized *a priori* volume geoelectrical model of Fennoscandia (Varentsov et al., 2002) were chosen as a reference data set (see more details in Section 6). The modelled impedance data have revealed a general agreement with the observations in a broad period range (Varentsov et al., 2002, 2003a,b). This agreement indicates, that most of the prominent large-scale anomalies in the spatial distributions of the observed data can be associated with known regional geoelectric structures.

However, an array-wide systematic shift in the impedance estimates (an array-scale source effect) cannot be detected in such a way because the modelling results depend upon the assumptions on the deep normal geoelectric structure. A special test of the regional impedance level in the long period range was based on the comparison of spatially averaged BEAR data with a number of global and European-scale MT/GDS references (Kovtun, 1989; Olsen, 1998; Semenov, 1998; Schmucker,

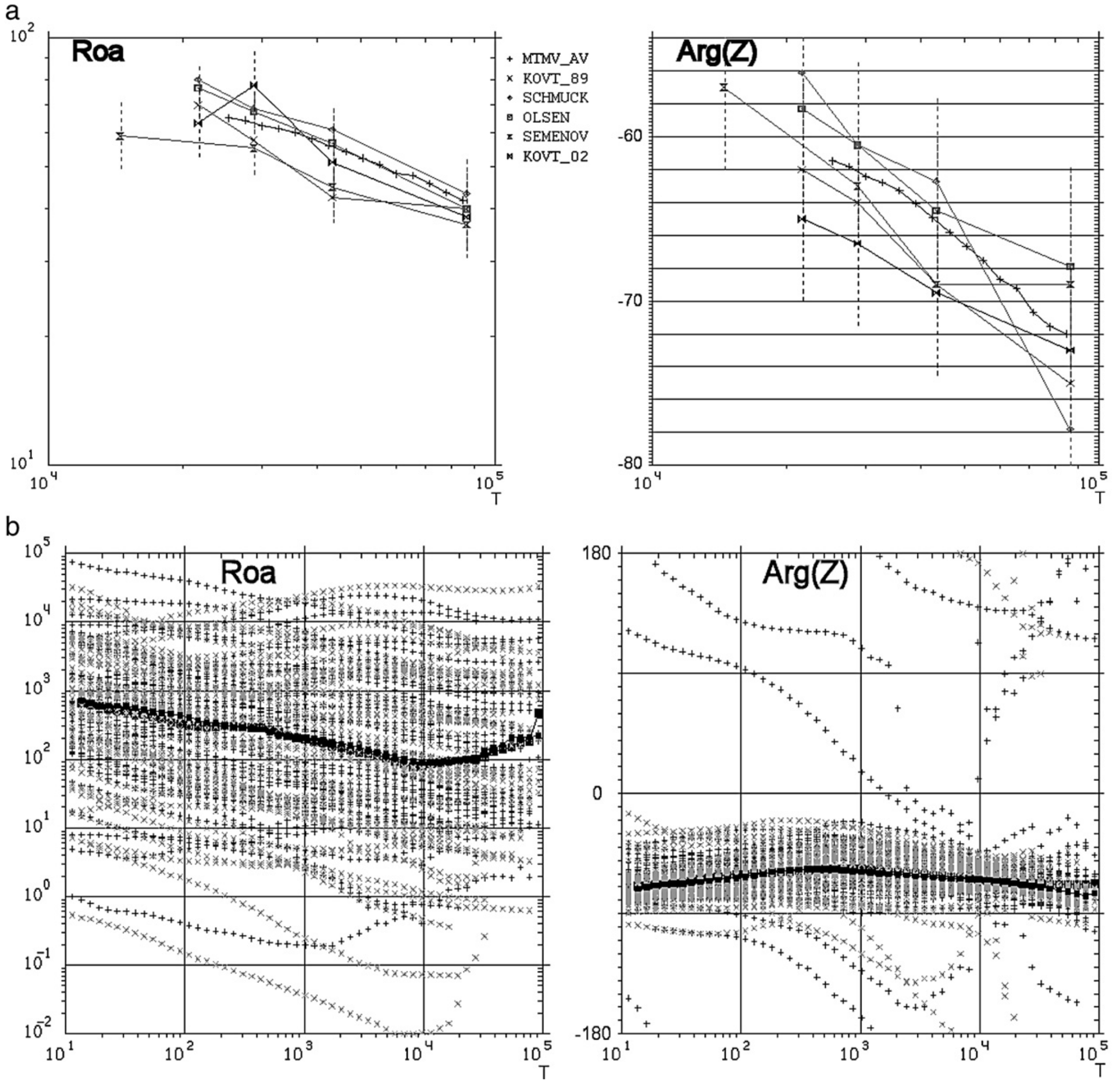

Fig. 6. a. The apparent resistivity (in Ω m, left) and the impedance phase (in degrees, right) for global and regional European MT/MV references at daily variation harmonics: KOVT_89 (Kovtun, 1989), SCHMUCK (Schmucker, 1999), OLSEN (Olsen, 1998), SEMENOV (Semenov, 1998); the result of their robust averaging, MTMV_AV, and the spatial average for the selected long-period BEAR sites, KOVT_02 (Kovtun et al., 2002). b. The spread of the apparent resistivity (left panel, in Ω m) and the impedance phase (right panel, in degrees) for all 44 sites of the BEAR experiment (dark and light crosses show *xy* and *yx* data components, respectively) and its medians (solid lines with black boxes) used for the construction of the BEAR_ALL spatial average response.

1999) at the daily variation harmonics (Fig. 6a). However, the scatter of shown references is quite large and in this comparison we prefer to use their formal robust average, marked in this figure as MTMV_AV.

The first spatial average of the BEAR data is based on the median analysis of principle impedance components in the original geomagnetic coordinate system (separate for amplitudes and phases) for the whole set (44 in total) of the BEAR MT sites (Varentsov et al., 2003b). The initial spread of these data and the estimated medians are shown in Fig. 6b. The spatial averaging of the apparent resistivity is no doubt a tricky procedure in the presence of strict static shifts typical at ancient shields. Actually, the apparent resistivity curves for the BEAR array scatter randomly for five decades without a distinct central cluster. The median averaging in this case is completely ineffective for periods greater than 4–5 h. However, it is an amazing fact that medians for *xy* and *yx* data components are fitting pretty well till the period of 3 h for the apparent resistivity and almost in the whole period range for the phase, where the misfit between two median curves becomes visible only at periods greater than 8 h. Thus, it seems quite natural to construct the effective array-wide impedance response, BEAR_ALL (Fig. 7), as an average of two close median estimates (*xy* and *yx*).

The median averaging approach was also applied separately for 22 northern and 22 southern BEAR sites, giving half-array average estimates BEAR_N and BEAR_S, correspondingly (Fig. 7, phase panel). The phase averaging results seem to be the most representative as based on consolidated enough ensemble of initial estimates (Fig. 6b, right panel). The first important observation is the good coincidence of the all-array (BEAR_ALL) and the half-array (BEAR_N and BEAR_S) averages within the misfit of 1–4° in the wide period range from first hundreds of seconds to one day. This misfit decreases with the period and becomes smaller than 2° at 2500 s and about 1° at daily variation harmonics. With such a fit at the periods, where the most pronounced source effects may be expected (Fig. 5), we hardly can assume the general increase in the scale of the impedance source distortions from the south to the north, predictable for inhomogeneous sub-polar sources. One may consider only the medium-scale mosaic effects modelled by Engels et al. (2002), which are sporadic in time and not strong enough to bias the half-array averages, based on the data from the whole experiment duration.

The second spatial average of the BEAR impedance data, KOVT_02 (Fig. 7), was constructed only at daily variation harmonics for a subset of MT sites with a good approach to global references in the longest period band (Kovtun et al., 2002). The fit of two different spatial averages (BEAR_ALL and KOVT_02) is quite good. The both phase responses are close to the lowest MT/GDS references and show a moderate divergence (about 5°) from the level of MTMV_AV average, being quite comparable with confidence intervals of initial references (Figs. 6, 7). This divergence becomes negligible approaching to the one day period. The KOVT_02 apparent resistivity looks consistent with the global/European references (Fig. 6, left panel) and approaches the BEAR_ALL average at the period of 4 h (Fig. 7, left panel). Thus, we see no significant array-wide bias in the BEAR average impedances at periods of daily variation range.

Maps of tipper coefficients and induction arrows at periods less then 3 h show reasonable agreement with 3D plane-wave modelled data, reflecting the known crustal induction anomalies. However, a strong northern deviation of the induction arrows and the dramatic increase of their amplitudes at periods greater then 3 h contradict the modelling data and presumably arise from the external source. Fig. 8 presents the plot of the induction arrows in the period range of 128–65536 s for the BEAR sites, located along the central BEAR 25°E meridian. The real arrows (given in the Wiese convention) point away from the conductors below the ground surface, but towards the external sources above it. The lengths of real induction arrows at periods below 3 h are generally small (about 0.1–0.2), but increase at sites close to pronounced crustal conductors (like the South Finland anomaly at the site B27 and the Oulu anomaly at sites B29 and B30) or towards the ocean (at sites B25, A06 and A09–A13). The azimuths of large arrows at these periods are well controlled by the strikes of the crustal conducting belts or the deep sea contours (Fig. 1). However, at periods greater than 3 h the real induction arrows are no longer dependent on local geoelectric conditions (even at sites B35 and A02 over the Lapland Granulate Belt), sharply increase in magnitude above the level of 0.5, and point in the N-NNW direction. These are the obvious signatures of the source effect. Only at the coast sites (A06, A09 and all Spitzbergen sites) with the most strong deep sea influence the external source effect is not dominating over the internal induction response.

The examination of the spatial-period behaviour of the BEAR local transfer functions gives grounds to conclude that the tipper data are almost free from the source distortions at periods below 2.5–3 h and that the “source–free” impedance estimation extends up to 6–8–12 and probably even 24 h at a number of favourable BEAR sites.

The ensemble of the BEAR inter-station transfer functions (Varentsov et al., 2003a,b) forms a unique data set constructed for the first time in such a large area. The

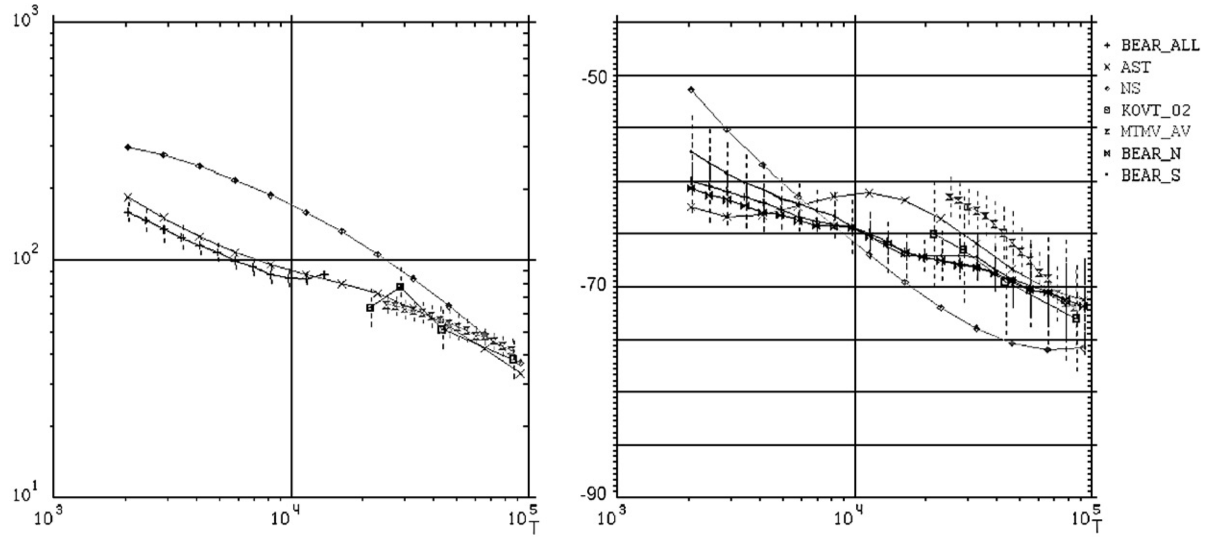

Fig. 7. The apparent resistivity (in Ω m, left) and the impedance phase (in degrees, right) curves for the robust spatial averages of all long-period BEAR data, BEAR_ALL, northern and southern array halves, BEAR _N and BEAR_S (Varentsov et al., 2003b) and the selection of BEAR sites, fitting well to magnetovariational references, KOVT_02 (Kovtun et al., 2002); responses for *a priori* BEAR deep 1D normal sections (NS and AST variants, without and with "asthenospheric" layer (see details in Fig. 12 and Table 1), according to Varentsov et al., 2002) and the robust average of global and regional MT/MV references, MTMV_AV (Fig. 6a).

analysis of their spatial-period structure in comparison with 3D modelling data (Varentsov et al., 2002) has shown that the behaviour of the horizontal magnetic tensor components in connection with the source influence is strictly different, than for the local TF responses. The amplitude components of this tensor are affected by the

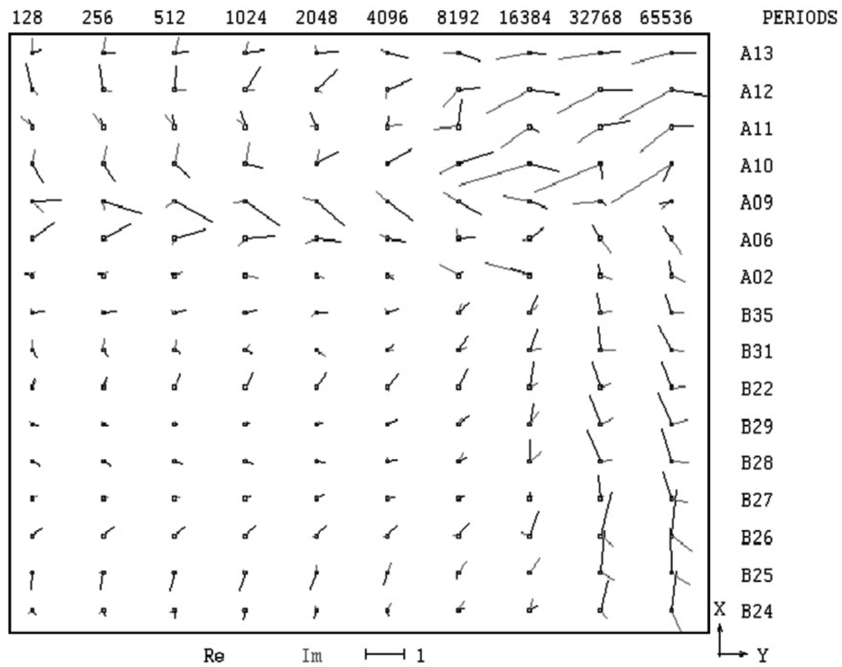

Fig. 8. The induction arrows (Wiese convention) along the central (25°E) meridian of the BEAR array (the real arrows in black and the imaginary ones in grey); periods (s) are given above each column of arrows, horizontal rows (from top to bottom) correspond to the particular BEAR sites, indicated in the right column from the North. (Spitzbergen) to the South (Estonia); the arrows are given in the coordinate system with the horizontal axis (Y) pointing to the East and the vertical (X) to the North; the scale bar gives a unit vector length.

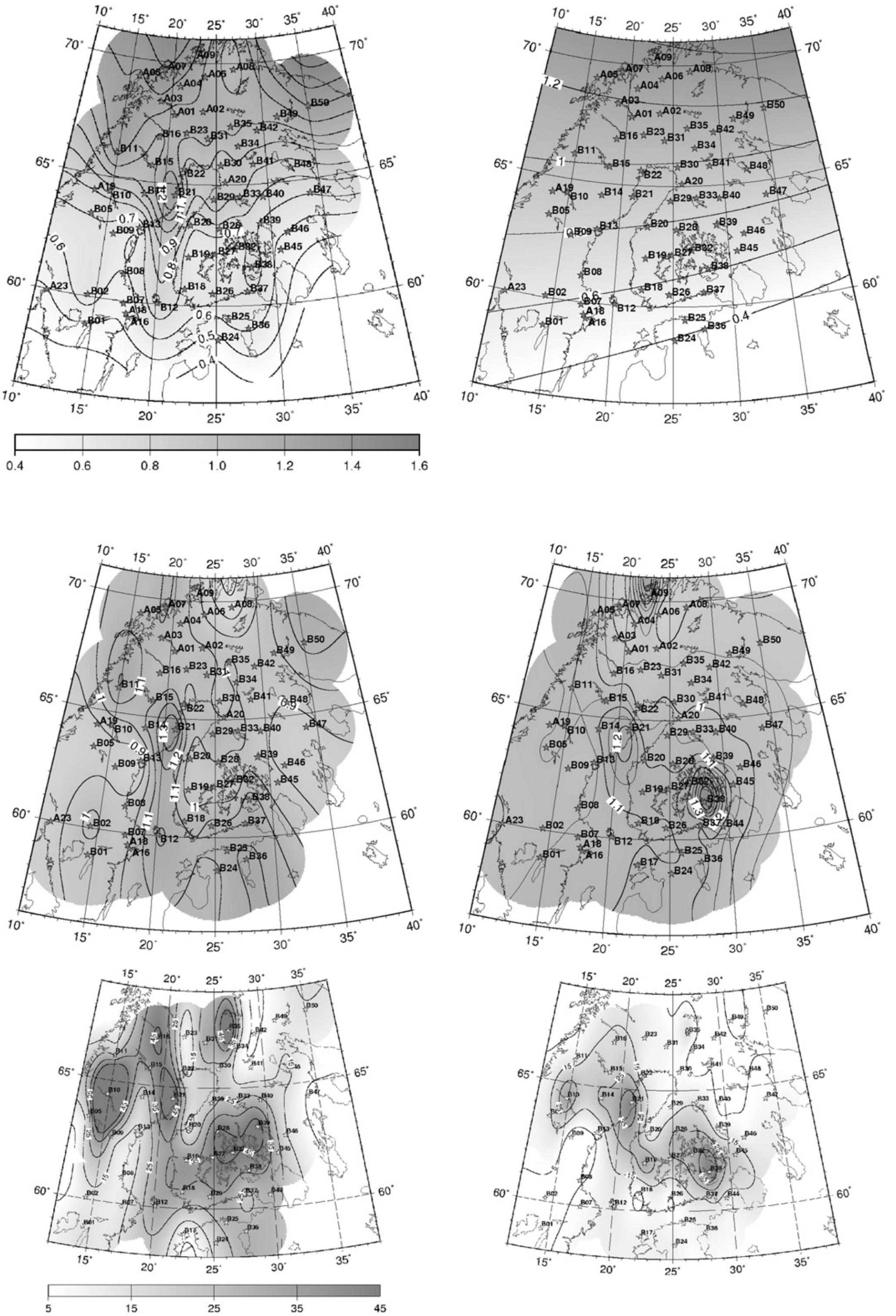

Fig. 9. The array maps of the BEAR transfer functions at the period of 2048 s: upper panels give horizontal magnetic tensor M_{xx} amplitude component (for the base site B22, left) and the estimated linear trend for it (right); middle panels show the remaining M_{xx} component after the trend subtraction (left) and the corresponding response, calculated in the BEAR volume model (Varentsov et al., 2002) with the AST normal section (Table 1); lower panels represent maps of the difference between maximal and minimal phase tensor invariants (the phase split) for the observed data (left) and those calculated in the volume model (right).

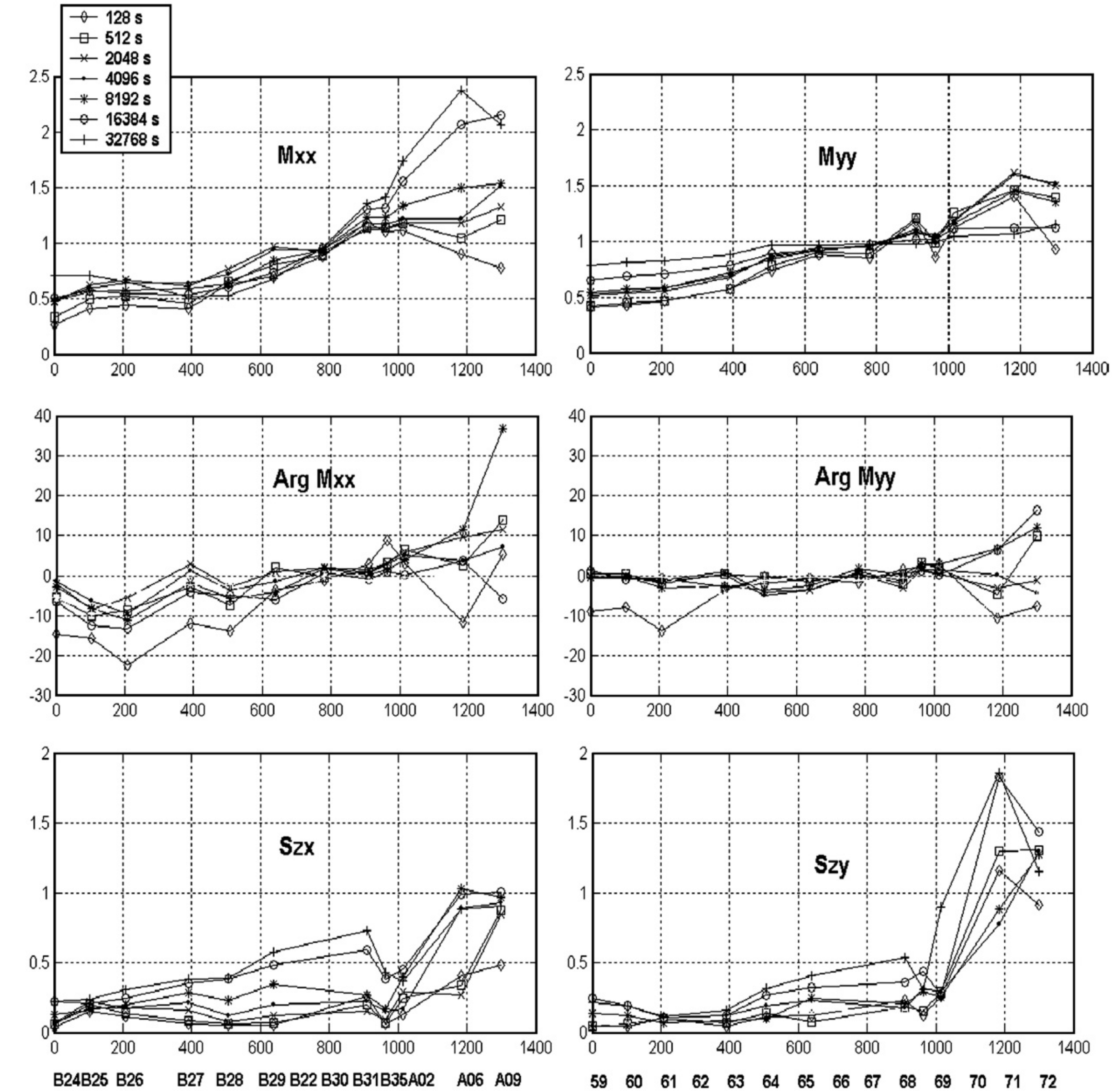

Fig. 10. The profiles of M_{xx}, M_{yy} (amplitude in relative units and phase in degrees) and S_{zx}, S_{zy} (amplitude in relative units) inter-station geomagnetic responses (relative to the base B22) along the central BEAR meridian (25°E) for a number of periods indicated in the legend; the horizontal axis gives the distance from the site B24 (km), site names and the geographical latitude (in degrees).

inhomogeneous source in a more broad period range than the tipper data. The evident northern trends are traced in M_{xx} and M_{yy} amplitude array-wide maps, while no such trends can be seen in 3D modelling responses. Fig. 9 shows in the left top panel the M_{xx} amplitude map at a period of 2048 s (here and below we consider estimates relative to the base B22). The observed amplitude obviously increases in the northern direction. The trend estimation procedure from the GMT toolkit (Wessel and Smith, 1998) outlines consistent bi-linear trends with NNW dominant gradient in the observed principle amplitude components (*xx* and *yy*). Such a trend in the M_{xx} component at 2048 s period is shown in the right top panel, and the residual data after the trend subtraction are given in the left middle panel. The amplitude trends are looking similar and changing quite smoothly with period from first hundreds of seconds up to the longest estimation periods, however, the spatial gradients for the M_{yy} data are some smaller. The modelled M_{xx} amplitudes (Varentsov et al., 2002), given in the right middle panel, exhibit the absence of any trends and demonstrate common patterns with the residual component of the observed data (left middle panel), in particular, the similar reflection of the major positive anomalies of the Bothnian–Ladoga crustal conductive zone.

The analysis of another inter-station $\mathbf{S_z}$ (regional tipper) data also has shown a general fit with the modelled responses at periods less then 2.5–3 h, while the maps of component amplitudes for periods above 3 h again demonstrate quasi-linear northern array-wide trends absent in 3D modelling images.

Fig. 10 presents another way to outline the spatial-period behaviour of the **M** and $\mathbf{S_z}$ inter-station data, showing graphs of their principle components along the central BEAR meridian (25°E) in the period range of 128–32768 s. The moderate effects of the crustal structures in the **M**-tensor amplitudes are superimposed by quasi-linear northern trends, being marginally stronger in the M_{xx} data. Smaller trends are also observed in the M_{yy} amplitude and M_{xx} phase profiles, but they are almost absent in the M_{yy} phase. The S_{zx} and S_{zy} amplitude profiles at periods of 100–10,000 s display quasi-homogeneous behaviour with the influence of the crustal conductors and the deep ocean coast effect. However, significant northern trends, presumably of external origin, appear in these responses at longer periods, being the most pronounced in the S_{zx} component with exception of the northernmost sites, subjected to the strong coast effect.

4. Experimental model of the external excitation for the BEAR array sounding

The analysis held in the previous section outlines the quasi-linear trends, which are present in the distributions of inter-station geomagnetic transfer functions in the wide period band over the whole BEAR array. The temporal stability and spatial-period pattern of these trends (in particular, their spatial gradients) give an assumption of an "effective" source of the BEAR sounding generalizing the actual excitation conditions. These TF data outlines a source located generally to north from the BEAR area, which produces geomagnetic field variations with stationary characteristics at the array-scale. The model of this inducing field assumes moderate N-NNW gradients in the horizontal components in the wide period range (from the first hundreds of seconds up to the longest periods of TF estimation) and the appearance of the vertical component with the same gradient direction at periods greater than 3 h. No local extremes are observed in this "effective" external field structure above the BEAR area. These conclusions are extended to the north from the continental BEAR area till Spitzbergen latitudes with the study of the longitudinal profiles of H_x and H_z robustly averaged spectra (Vanyan et al., 2002b; Varentsov et al., 2003b).

This pattern characterizes the external excitation conditions for the whole duration of the experiment and reflects both the accumulation of the distant source influences, and the absence of visible superposition effects from inhomogeneous source events within the array, including the nearest electrojets. Moreover, this model demonstrates the measure of temporal and spatial averaging over different sources in the TF estimation course, and corresponds to the final ensemble of the BEAR transfer functions.

The geophysical understanding of the constructed effective source model comes from the specific structure of the ionospheric and magnetospheric current systems in the summer of 1998 (Vanyan et al., 2002a; Levitin et al., 2007). The effective pattern of these current systems for the BEAR observation time was determined in these studies according to the IZMEM magnetic field model (Feldshtein and Levitin, 1986) with an account for simultaneous ground EM observations and satellite data, supplying the most probable interplanetary magnetic field parameters in the vicinity of the Earth's orbit. The maximal current density zone in the constructed equivalent ionospheric current systems was typically located far away from the array in the polar cup area (Fig. 11) and produced quasi-linear spatial changes in the geomagnetic field above the array. These model assumptions substantially differ from the earlier adopted view on the external sources in Fennoscandian high latitudes (for example,

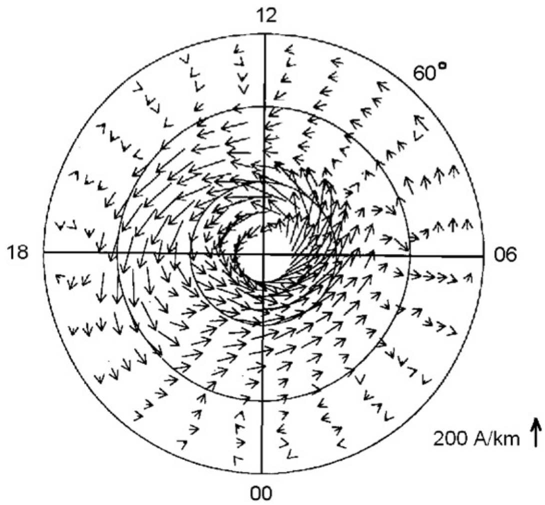

Fig. 11. The typical spatial distribution of the equivalent ionospheric current system in the northern polar cap (in magnetic local time, for latitudes from 60° to 90°) during the BEAR experiment in June–July, 1998 (Levitin et al., 2007); the vector in right bottom corner gives the scale for current magnitude (A/km).

Osipova et al., 1989), characterized by dominating effects of the auroral electrojets with high gradients and extremes in the magnetic field spatial distribution near the Polar circle. The models of Levitin et al. (2007) with dominating polar cup currents correspond well to the presented above pattern of the effective external geomagnetic source inferred from the BEAR two-month averaged TF responses.

5. The validity of the plane wave assumption for the BEAR sounding data interpretation

The understanding of the actual excitation conditions in every specific EM sounding is required for checking the validity of the traditional MT/GDS sounding paradigm and the selection of adequate modelling and interpretation techniques. The widely adopted excitation model for the natural EM field soundings (Weidelt, 1978; Dmitriev and Berdichevsky, 1979) extends the margins of Tikhonov–Cagniard classical plane-wave assumption and permits linear changes in the horizontal components of the external geomagnetic field. More complex spatial patterns of the primary field may ruin the TF invariance to the source parameters, on which their further interpretation is usually based. Moreover, in the presence of sufficient H_z component in the primary field the traditional four component impedance linear relationships may become ineffective, requiring additional account for the vertical magnetic field in the construction of generalized 6-component impedance tensor (Dmitriev and Berdichevsky, 2002).

This problem is of great importance for the BEAR upper mantle studies, because the period range of the most pronounced effects of inhomogeneous sub-polar sources on the TF data (1500–10,000 s, Figs. 3, 5) corresponds to the exploration depth range of about 200–300 km as seen both from simple effective wavelength estimates or more accurate model calculations (Section 6). Fortunately, the effective source model of the BEAR sounding gives a solid background for the interpretation of the impedance and tipper data in this period range within the conventional plane-wave excited models. The effective source model till periods about 3 h does not reveal significant non-linear spatial effects in the horizontal magnetic field and is characterized by negligibly small vertical external magnetic field, while the coherence in the impedance and tipper estimation is generally high and their estimates exhibit a prominent temporal stability. However, the conventional interpretation of tippers at periods longer then 3 h will be definitely misleading.

The mutual coherence of the impedances at many BEAR sites continues to be sufficiently high well above the period of 3 h giving grounds to extend the limits for the cautious use of plane-wave impedance interpretation models. This extension of the period range is supported by appropriate correspondence of BEAR MT data to the global and regional MT/GDS references at daily variation harmonics and by the good fit between array and half-array long period phase averages (Fig. 7). We still see some resources for the "source-free" impedance and tipper estimation at periods greater then 3 h on the way of selecting the temporal events with the limited norm of partial tipper estimates as suggested by Jones and Spratt (2002). The close idea to reject time events with partial tipper estimates being far from the final sorted and averaged response is suggested by Ernst and Jankowski (2005). Another way is to apply a number of sorting criterions on the partial estimates of the horizontal magnetic tensor, proved in the elimination of strict train effects in Polish Pomerania (Sokolova et al., 2006). All these resources originate in the multi-site observation schemes and joint analysis of partial estimates for different transfer functions to provide effective event rejection criteria. An effective alternative to the conventional MT approach in the mantle studies may be the joint horizontal spatial gradient (HSG) and GDS method (Schmucker, 2003; Korja and Smirnov, 2006).

Finally, it should be stressed that the traditional plane-wave interpretation of the BEAR horizontal magnetic tensor data (almost in the whole period range of TF estimation correspondent to the crustal and mantle depths) requires the separation into the external and internal parts at least in the form of the simplest quasi-linear trend reduction (Fig. 9) or by means of more sophisticated approaches.

6. Implications for the study of the Baltic Shield upper mantle conductivity

In this section we describe preliminary geoelectric models of the lithosphere–asthenosphere transition beneath the Fennoscandia derived from the BEAR data and examine the reliability of these results and, in particular, their dependence on the data uncertainties related to the inhomogeneous source influence.

The first indication on the existence of the upper mantle conductive structure (the electrical "asthenosphere") under the studied area from the BEAR data was found in the comparison of the observations with quasi-3D and volume 3D modelling results (Engels et al., 2002; Varentsov et al., 2002). Both modelling approaches were based on the multi-sheet crustal conductance model (SMAP) (Korja et al., 2002), which integrates available *a priori* information over the whole Fennoscandia and its

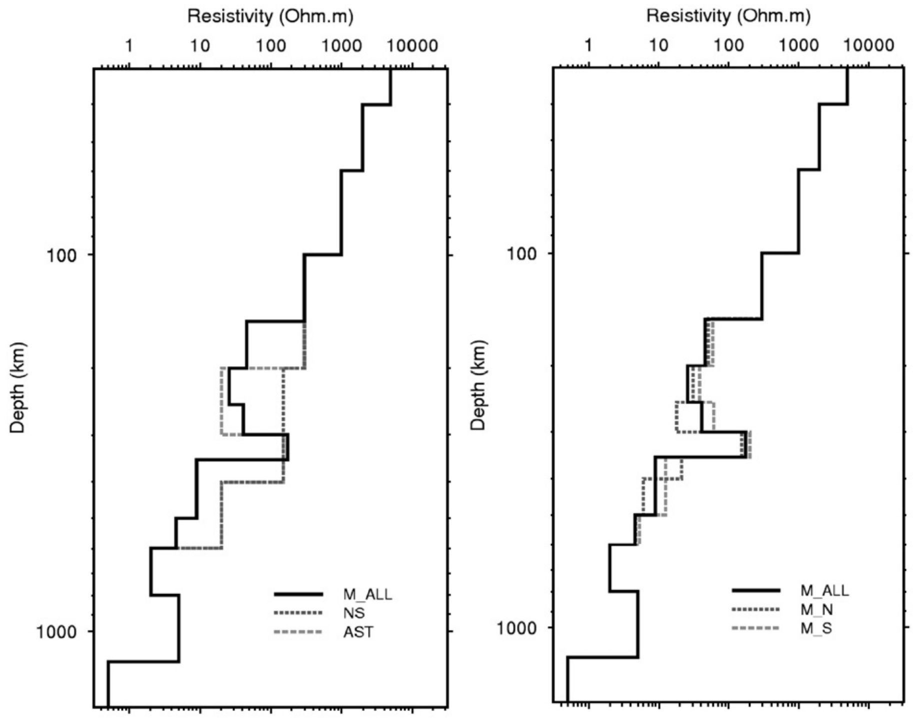

Fig. 12. 1D deep resistivity profiles (Ω m) versus depth (km) in bi-logarithmic scale derived in the BEAR experiment, left panel: from the BEAR volume conductivity model (Varentsov et al., 2002) without (NS) and with (AST) conducting "asthenospheric" layer (5000 S at 200–300 km depth) and for 1D model with gradient "asthenospheric" resistivity distribution (M_ALL, 4200 S at 150–300 km depth), fitting the average impedance BEAR_ALL; right panel: 1D model M_ALL compared with models M_N and M_S, obtained in the same way by 1D fitting of northern and southern half-array average responses, BEAR_N and BEAR_S (see also Fig. 7, Table 1).

surroundings, and on the regional 1D deep normal section applied below the crust and at the edges of the SMAP construction. This normal section generalizes (Korja et al., 2002) the variety of known 1D conductivity distributions derived independently at different parts of the BEAR region and from a number of shield-wide and global conductivity profiles. Two isotropic normal section variants, namely the resistive profile, NS, and the profile with an "asthenospheric" conducting layer with a 5000 S conductance at 200–300 km depth, AST (Figs. 7, 12, Table 1), were considered in these 3D simulations. The shield-wide "asthenospheric" hypothesis, expressed in the AST normal section, looked preferable in the comparison of the observed and modelled impedance phases (Engels et al., 2002; Varentsov et al., 2002).

The latter paper presents an important for our analysis data sensitivity study, based on the comparison of two accurately calculated alternative 3D modelling responses,

Table 1
Alternative 1D normal resistivity models related to the BEAR EM sounding data (Figs. 12, 13)

Model	Depth to the top (km)	0	10	20	30	40	60	100	150	200	250	300	350	400	500	600	800	1200
	Thickness (km)	10	10	10	10	20	40	50	50	50	50	50	50	100	100	200	400	
NS	Resistivity (Ω m)	40	20000	10000	5000	2000	1000	300	300	150	150	150	150	20	20	2	5	.5
AST	Resistivity (Ω m)	40	20000	10000	5000	2000	1000	300	300	**20**	**20**	150	150	20	20	2	5	.5
M_ALL	Resistivity (Ω m)	40	5000	5000	5000	2000	1000	300	**46**	**26**	**41**	174	**8.9**	**8.9**	**4.6**	2	5	.5
M_N	Resistivity (Ω m)	40	5000	5000	5000	2000	1000	300	**51**	**31**	**18**	154	**21**	**6**	**4.7**	2	5	.5
M_S	Resistivity (Ω m)	40	5000	5000	5000	2000	1000	300	**59**	**38**	**61**	202	**12.6**	**12.6**	**5.3**	2	5	.5

Notes: NS and AST — normal sections used in the BEAR volume conductivity model (Varentsov et al., 2002), without and with conducting "asthenospheric" layer (5000 S at 200–300 km depth); M_ALL — model with a gradient "asthenospheric" conductivity distribution (4230 S at 150–300 km depth), fitting the average BEAR_ALL impedance response; M_N and M_S-models with conductances of 5370 and 2980 S at 150–300 km depth, which fit half-array average data (BEAR_N and BEAR_S), correspondently; the significant discrepancies of AST and other models from the NS profile are outlined in bold.

Table 2
Relative misfit norms over the array area (in %) of the residuals between plane-wave 3D modelling responses for the BEAR volume conductivity models with and without conducting "asthenospheric" layer (5000 S, 200–300 km depth) for different transfer functions ($\boldsymbol{Z}_{\mathrm{eff}}$ and $\rho^{\mathrm{a}}_{\mathrm{eff}}$ — the square determinant impedance and the correspondent apparent resistivity, $\boldsymbol{W}$ — induction arrow) at different periods (according to Varentsov et al., 2002)

Period (s)	32768	16384	8192	4096	2048	1024	512	256	128
Log-Amp ($\rho^{\mathrm{a}}_{\mathrm{eff}}$)	8.09	13.0	**15.4**	12.2	6.82	2.37	1.14	1.06	0.51
Phase ($\boldsymbol{Z}_{\mathrm{eff}}$)	**45.7**	**27.1**	7.18	19.8	**25.6**	**22.1**	12.7	5.74	1.07
Amp (Re $\boldsymbol{W}$)	12.1	7.39	**20.1**	**19.7**	14.1	5.72	3.13	2.28	1.42
Amp (Im $\boldsymbol{W}$)	12.4	**20.9**	**22.6**	15.5	**29.1**	**28.4**	15.2	12.1	2.05

Notes: The increased misfit norms indicating the maximal data sensitivity to the upper mantle conductivity at 200–300 km depth are printed in bold.

obtained in volume crustal models with NS and AST normal sections. Table 2 gives the resulting shield-wide relative misfit norms for a number of principle data components in a broad period range and makes possible to compare "asthenospheric" anomalies in different components and to search for their extremes with a period. In general, these anomalies exceed the level of 20–30% relative to the spatial variation of considered components within the whole array area. In particular, this table shows that the best general (spatially averaged) sensitivity for the regional "asthenospheric" layer (5000 S at 200–300 km depth) occurs at periods of 1.5–4 h for the apparent resistivity data, while for the impedance phase two peaks appear at periods about half an hour and 6–12 h; the length of the real induction arrow has a maximal sensitivity at 1–2 h and the length of the imaginary induction arrow again has two separated peaks at periods of 15–45 min and 2–5 h. These estimates, taking into account the inhomogeneous crustal structure, indicate the necessity for the complex interpretation of different TF responses, which are most sensitive to the upper mantle conductor in different period ranges, and give a reasonable optimism for the resolution of this target in the specific Fennoscandian conditions. In fact, in a view of the constructed effective excitation model only the second resolution peak of the imaginary induction arrow is seriously contaminated by source effects, as for the second impedance phase peak, we have grounds for the meaningful interpretation of carefully selected extra long period phase responses (Section 3).

The analysis of 3D modelling data outlined within the BEAR array several areas with homogeneous enough long period impedance responses (Varentsov et al., 2002), namely, Southern Sweden, Central Lapland, Karelia and, finally, Estonia and Southern Finland. These areas were of primary interest for the application of conventional 1D data interpretation approaches. Vanyan et al. (2002a,b) presented 1D inversion results for the BEAR sites in Central Lapland, averaging impedance data over small clusters of sites and inverting average impedance components, being the closest to global references. This approach gives upper mantle models with a conducting layer (30 Ω m) appearing at depths about 250 km. Kovtun et al. (2002) made quite similar 1D interpretation separately for a larger set of BEAR sites with small 3D distortion parameters (skews). The dominant type of models in this analysis, made with an emphasize of the phase responses, also contained rather sharp resistivity decrease to a level of 20–50 Ω m at a depth greater than 200 km. Recently Lahti et al. (2005) published results of a detailed 1D inversion study at the BEAR site B42 in Eastern Lapland, held together with few close audio-MT soundings. The site B42 was selected as one of the most suitable for 1D treatment on the base of detailed decomposition analysis. The inversion of the combined audio-MT and long period MT impedance determinant data (up to the period of 3 h) indicates a sharp resistivity decrease to the level of 10 Ω m at 170 km depth, reflected in the data for periods above 300 s (phase) and above 2000 s (apparent resistivity). Our experiments with the same data, but using the robust 1D technique (Varentsov, 2002) and emphasizing phase responses, give some greater depths (200–240 km) and resistivities (~20 Ω m) for this "asthenospheric" jump. These preliminary results of the BEAR data 1D interpretation are in a good agreement with the inferences of Jones et al. (1983) on the conductive upper mantle structures under Fennoscandia, obtained on the limited but carefully selected (against the source influence) data set.

It is possible to conclude, that the excessive upper mantle conductivity seems to be a regional feature for the whole BEAR region, but its 1D resolution is seriously masked by local crustal structures. Further we concentrate on the 1D inversion of the array-wide average impedance response BEAR_ALL (Fig. 7), which gives a better rid of inhomogeneous crustal effects and better outlines common regularities in the resistivity profile, most important in our resolution study. This inversion was focused on the phase BEAR_ALL response in the period range from 1400 s to 24 h (Fig. 13), while the correspondent apparent resistivity data were taken strictly downweighted in the limited range of 1400–10,000 s. At the first inversion stage the phase data were jointly fitted with apparent resistivities, but then the variability of the crustal part of the resulting model was limited and the inversion continued with fitting only the phase data, thus concentrating on the upper mantle resolution. The model M_ALL obtained in this way is presented in Fig. 12 and Table 1. It contains an "asthenospheric" conducting layer at 150–300 km depth with the total conductance of 4230 S and the lowest central resistivity of 26 Ω m with more resistive edges slightly above 40 Ω m. This model also has less resistive profile at depth below 350 km comparing with NS and AST models (Fig. 12, Table 1), but in the depth range of 300–350 km its resistivity is above 170 Ω m, marking the bottom of the "asthenospheric" layer. The data fit is very good (about 1°) for the phase data and looks quite acceptable for the downweighted apparent resistivity (Fig. 13a). The conductance of the outlined "asthenospheric" layer (4230 S) is slightly less than the previous 3D modelling estimate (5000 S), while the "trapezoid" resistivity profile may represent both the smooth resistivity change at the top and bottom edges of this layer or the spatially averaged variation of edge depths.

The model M_ALL mainly represents the array-averaged impedance phase data, which look free from source distortions and minimize the influence of crustal

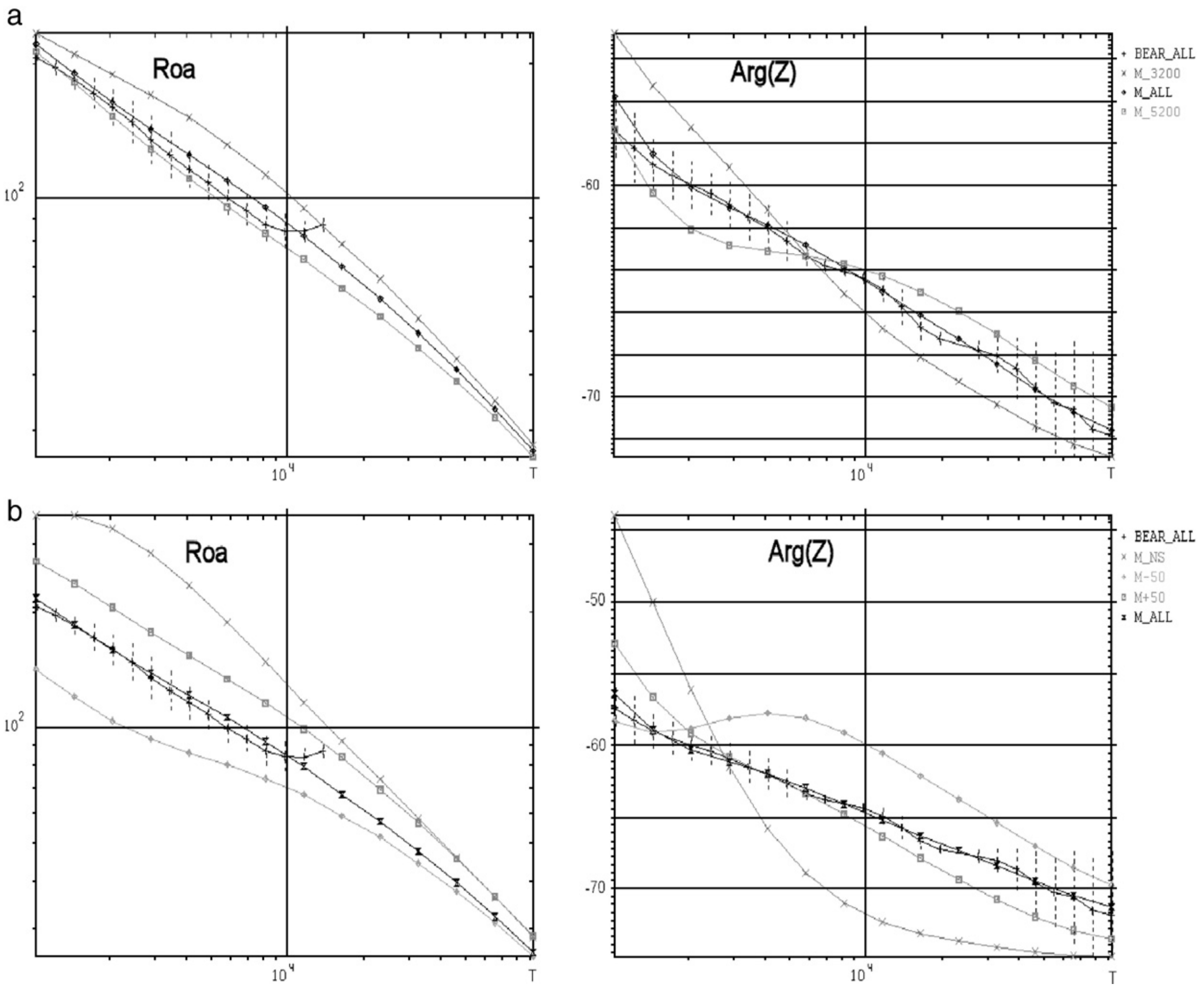

Fig. 13. a. The comparison of the spatial average of long-period BEAR impedance data BEAR_ALL with 1D model response for the model M_ALL, which fits this average, and two related responses, M_3200 and M_5200, for models with 1000 S conductance perturbation at 150–300 km depth from the level of M_ALL model (~4200 S); left panel — apparent resistivity (Ω m), right panel — phases (degrees). b. The comparison of the spatial average of long-period BEAR impedance data BEAR_ALL with 1D model response for the model M_ALL, which fits this average; two related responses, M + 50 and M − 50, for models with 50 km perturbation of the depth to the top of "asthenospheric" layer from the level of M_ALL model (150 km) and the response M_NS, which corresponds to M_ALL model with completely excluded "asthenospheric" layer; left panel — apparent resistivity (Ω m), right panel — phases (degrees).

effects, and in this respect it gives additional support for the hypothesis of a wide presence of the "electrical" asthenosphere below the Fennoscandia. This solution looks as a useful frame for our current tests of asthenosphere resolution and can be further used as a background model in the 3D inversion study.

The presented investigation of the BEAR sounding effective source and the TF data temporal stability, showing generally source-undistorted character of the impedance and tipper estimates in the period range up to 3 h, proves the possibility of their trustworthy inversion in models with a plane-wave excitation. The 1D modelling analysis shows, that for the 3-hour boundary of this confident period interval the exploration depth of the MT sounding ranges around 300 km depending on the crustal conductance and the deep normal section assumptions used, while the use of MT data up to the 1 day period extends the exploration depth to about 600 km. The "asthenospheric" effect is clearly distinguished in 1D modelling responses for AST and M_ALL resistivity profiles in comparison with the data for the NS model in the period range from hundreds of seconds to 24 h (Figs. 7, 13a, b). The first extreme of the AST impedance phase curve at 1800–3000 s gives the signature of the top edge depth of the conducting layer, while the second extreme above 3 h characterizes its bottom edge depth. The difference of these phase peaks and the apparent resistivity anomaly (maximal at 1–3 h) are mainly dependent on the layer conductance, being a ratio of its thickness to resistivity. These data sensitivity issues explain the lack of resolution for the bottom of the "asthenospheric" layer from the single site 1D inversions with significant data quality decrease at the longest periods and its quite clear indication in the model M_ALL, derived from the array-wide average response with a greater stability at periods above 3 h. The models M_N and M_S (Table 1), derived in the same way as the model M_ALL, but from the half-array average responses BEAR_N and BEAR_S (Fig. 7), demonstrate the same top and bottom edges of the "asthenospheric" conducting layer and the variance in its conductance from 2980 to 5370 S for southern and northern half-arrays, respectively. Note, however, that the southern average, BEAR_S, has larger estimation errors due to the greater influence of the crustal inhomogeneity (especially, in Central and Southern Finland, Fig. 1) and thus the "asthenospheric" conductance for the model M_S looks less reliable.

The useful estimates of the resolution limits for the upper mantle conducting structures and, in particular, for the parameters of the "asthenospheric" layer may be obtained in the comparison of the variability of related MT responses with a measure of the data uncertainty. The data processing error estimates for the impedance are defined in average for the period range of 8–10,000 s and almost all of the BEAR sites at the level below 2° for the phase, 4% for the amplitude and 8% for the apparent resistivity (Varentsov et al., 2003a). These error estimates should incorporate most of the random disturbing factors, including the source inhomogeneity.

The estimation of the bias (systematic error) scale for the impedance data is a more difficult task. We assume that the major contribution here comes from the source inhomogeneity, not considering temperature and electrode effects. The upper bound of this bias (tens of degrees in the impedance phase) may be seen in static model of the electrojet source (Osipova et al., 1989) or in the "exotic" TF estimates (like STORMS and even No_Coh_S in Fig. 5), obtained without the elimination of strongly source-distorted time events. However, these bounds were proved to be strongly overestimated in previous sections of this paper. Quite a realistic bias estimate, being well below 2° in the phase at periods greater 2000 s, comes from the comparison of the array/half-array average impedance responses, BEAR_ALL, BEAR_N and BEAR_S, (Fig. 7) and seems to be within the scale of data uncertainties of a random nature.

With the account for the scale of data uncertainties we demonstrate changes in the apparent resistivity and phase responses for the model M_ALL with perturbations both in the "asthenospheric" conductance (Fig. 13a) and the top edge depth (Fig. 13b). The conductance perturbation in the range of 4200±1000 S (M_3200 and M_5200 responses in Fig. 13a) changes quite symmetrically the phase data for 2–3° and the apparent resistivity for about 10%. The depth perturbation effects in the phase look less symmetric (Fig. 13b). The shallow position of the "asthenospheric" layer (M−50 model with 50 km higher top edge) gives greater changes, especially, at 1–3-hour periods (8–10°) than for the alternative perturbation (M+50 model with 50 km deeper top edge) with changes below 5° in the whole period range. The apparent resistivity changes in this case are more compatible (~20% at the 3-hour period). The general conclusion from this variability analysis is that the BEAR impedance data with the estimated uncertainty level may resolve the changes at least of 1000 S in the "asthenospheric" layer conductance and of first tens of km in its top edge depth. Fig. 13b also shows the response M_NS for the M_ALL model with completely excluded "asthenospheric" layer. The effect of this exclusion is drastical and counts for more than 40% in the apparent resistivity and more than 10° in the phase in almost the whole period range. This difference is at least 4–5 times greater than the data uncertainty.

The derived conclusions on the resolution bounds for the upper mantle conducting anomalies in relation to the BEAR impedance data took into account isotropic geoelectric models and may not be true in models with significant conductivity anisotropy. Bahr and Simpson (2002) justified the anisotropic upper mantle conductivity structure below the Fennoscandia (in particular, in Central Finland), basing on the strong (above 40°) impedance phase split (the difference between maximal and minimal phase invariants) and regionally stable strike directions at long (above 1000 s) periods as well as the absence of visible correlation between spatial patterns of the phase split and the horizontal magnetic tensor amplitudes. At the same time, the careful 3D modelling analysis explains the observed strike directions and phase split anomalies almost completely by the known crustal heterogeneities (Varentsov et al., 2002; Lahti et al., 2005). Fig. 9 (bottom panels) shows maps of the observed phase split, calculated from the phase tensor invariants (Caldwell et al., 2004), and of the same response, calculated at all the BEAR sites in the volume model of the Baltic Shield (Varentsov et al., 2002) at the period of 2048 s with an exploration depth about 200 km. The modelled phase split in *a priori* geoelectric model (without any account for the BEAR data) extends the level of 35° and explains more than 80% of the observed anomalies. Surely, this fit may be improved with the optimization of this model. Thus, the phase split factor is not a serious argument for the upper mantle anisotropy. As for the evidence from the horizontal magnetic tensor data, we proved in Section 3, that the stationary source influence made them untreatable for the study of geoelectric structure before the proper internal part separation. Fig. 9 also shows for the same period of 2048 s, that after the simplest internal part separation in the form of the amplitude quasi-linear trend subtraction (Varentsov et al., 2003b) the residual amplitude pattern (left middle panel) displays quite an obvious correlation with the phase split structure (left bottom panel). This example demonstrates how the accurate modelling analysis and the careful investigation of the source distortions oppose the importance of the upper mantle anisotropy assumption. However, we shouldn't reject it completely and may return to its investigation after reaching a proper fit in the isotropic crustal–mantle 3D model of the BEAR experiment.

The interpretation of the BEAR transfer functions, carried out by different project teams is in the progress. Its tasks are concentrated around two separate poles of quasi-1D and full 3D inversion studies. The foregoing discussion gives better grounds and limits for the use of plane wave interpretational models in this work. The main task of 3D inversion outlined by Varentsov et al. (2002) is to examine the spatial and depth variation of the excessive upper mantle conductivity, evaluated above in a 1D approach, using the smooth finite function approximation (Varentsov, 2002) and accepting with minor changes *a priori* crustal 3D structure. This approach provides the joint fit of a wide ensemble of different long period TF data components taking into account the period range and component type limitations originated from the general data accuracy and sensitivity estimates as well as from the specific knowledge of available source distortions. The discussed above resolution and data sensitivity issues give grounds to expect the reconstruction in the course of 3D inversion of a smooth electrical asthenosphere pattern under the Fennoscandia with characteristic lateral dimensions greater than 300–400 km.

At the current stage there are several hypotheses on the nature of the electrical asthenosphere in Fennoscandia. Lahti et al. (2005) related the enhanced upper mantel conductivity with the partial melt or hydrogen diffusion processes according to (Karato, 1990). Kukkonen et al. (2003) suggest the lithosphere/asthenosphere boundary at the depth of 200–250 km, accept the wet rheology with a percent-level fluid content, but have doubts on the beginning of the partial melt in the Fennoscandian asthenosphere: the fluid content is high enough to allow for wet rheology, but apparently may be too low to start the partial melting. Kovtun et al. (2002) relate the conductivity increase at depth about 200 km to the transition to the intrinsic ionic conductivity in specific pressure conditions.

Gordienko (2001) outlined a number of areas of recent activization within the Baltic Shield and its slopes, basing on the complex of geophysical (non-electromagnetic) methods. These areas correlate quite well with the regions of modern sedimentation in the Bothnian and Finnish Bays of the Baltic Sea and the Kandalaksha Bay of the White Sea, including the adjacent land, and permit the existence of mantle partial (2–5%) melting zones with a resistivity being as low as 30 Ω m within a thickness up to 75 km. The latter estimates correspond well to the most conducting layer of the M_ALL model (Table 1) with the resistivity of 26 Ω m and the thickness of 50 km, while the location of these areas is close to a number of blocks with the increased upper mantle conductivity (Southern Lapland, North-Eastern Karelia, the coast of the Finnish Bay, North-Eastern Sweden), outlined in the 1D inversion analysis of the BEAR data (Vanyan et al., 2002a,b; Kovtun et al., 2002; Lahti et al., 2005).

The recent seismo-tomographic SVEKALAPKO array in Central and Southern Finland gives generally normal upper mantle state (Sandoval et al., 2004) with maximal anomalous effects at the array edges with a natural lack of resolution. However, at the moment no serious contradictions occur with the BEAR geoelectric models, because the most prominent indications on the electrically anomalous upper mantle take place outside the seismic array, while the mantle conductivity structure in Central Finland is hidden by the influence of the strongest crustal conducting belts (Korja et al., 2002) and cannot be revealed without sophisticated 3D inversion and, probably, further more detailed EM soundings. Moreover, the correlation between the upper mantle low resistivity and low seismic velocity may be traced at the Swedish coast of the Bothnian Bay and the Estonian coast of the Finnish Bay.

We would like to postpone a more detailed discussion of the nature of the excessive upper mantle conductivity below the Fennoscandia before getting reliable 3D inversion results for the BEAR data, which should bring better vision of its spatial and depth structure.

7. Conclusions

The experimental model of the external excitation for the BEAR array sounding, effective for the whole period of observations, is presented. It is characterized by quasi-linear changes in the primary geomagnetic field over the array with the correspondent vertical component becoming noticeable at periods above 3 h. This model is consistent with the robustly estimated TF data ensemble, serving for the reconstruction of the deep geoelectric structure of the Baltic Shield.

The validity of the plane wave approach in the interpretation of the BEAR transfer functions is justified for the impedance and tipper data at least till periods below 3 h, as follows from the spatial-period structure of the "effective" external source. At the same time this approach is inapplicable for the horizontal magnetic tensor data in the whole long period range and the direct use of these data for the resolution of the deep geoelectric structure may be seriously misleading. The BEAR impedance data at periods greater than 3 h, especially phases, contain valuable information on the "deep roots" of the upper mantle conductivity structure. The spatially averaged BEAR impedance estimate in the daily variation period range appropriately corresponds to the global and European-scale MT/GDS references and to this extent may be regarded as having passed the "first-order" testing. However, these extra long period data, probably, should be further examined in relation to the external source distortions, in particular, to the influence of the vertical external field. The horizontal magnetic tensor responses as well as the extra long period tipper data require the separation of their internal parts to be interpreted within the plane wave approach. The application of the horizontal spatial gradient (HSG) technique or the joint HSG/GDS method (Schmucker, 2003) to these data in the specific Baltic Shield areas might be reasonable alternative to the direct internal parts separation.

The present understanding of the Fennoscandian upper mantle geoelectric structure derived from the BEAR data mainly comes from their comparison with generalized 3D simulation results and conventional 1D inversion of the MT data, both outlined the general increase of the conductivity at the depth greater than 150–200 km in comparison with *a priori* resistive deep normal profile NS. These signatures of the lithosphere–asthenosphere transition under the Baltic Shield deserve a sufficient confidence as traced in the impedance and tipper responses at the periods from first hundreds to first hours, where source effects are shown to be negligible and the overall data accuracy is high. The enhanced conductance at the 150–300 km depth reaches the level of 4000–5000 S and can be expressed, taking into account the limits of 1D resolution, both as an "asthenospheric" conducting layer with further monotonous resistivity decrease or as an earlier and sharp decrease in the resistivity profile. The presented 1D inversion results for the spatially averaged whole array (half-array) long period impedance responses look closer to models of the first kind.

The crustal inhomogeneity of the Baltic Shield gave no success in the use of 2D inversion techniques within the whole lithosphere. The specific 3D inversion of the long period BEAR data for smoothly parameterized upper mantle conductivity variations and almost fixed *a priori* crustal structure (Varentsov et al., 2002) is on the way and may bring better reconstruction of the lithosphere–asthenosphere transition.

The current study, summarizing the broad experience in the treatment of the source effects in the BEAR array data and focusing on the understanding of the MT/GDS sounding effective excitation model, helps to elaborate the adequate methodology for the long period data analysis in this particular experiment and yields new insight on the general applicability of natural EM sounding methods in the sub-polar areas.

Acknowledgments

We thank the BEAR Working Group teams for the fruitful collaboration, and, personally, M. Engels, T. Korja, S.-E. Hjelt, A.A. Kovtun, I. Lahti, N.A. Palshin, L. Pedersen, M.Yu. Smirnov. We outline a remarkable role in the project of untimely gone L.L. Vanyan and are grateful to A.E. Levitin for the study of the polar ionospherere–magnetosphere current system, justifying our model of the effective source for the BEAR sounding. We finally thank our reviewers for their important suggestions improving the manuscript. This work was supported by the following grants: INTAS 97-1162; RFBR 98-05-65411 and 03-05-64646; and the EUROPROBE/SVEKALAPKO research program.

References

BEAR Working Group, 1999. BEAR is searching into a lithosphere–asthenosphere boundary beneath Fennoscandia. Proc. of 4th SVEKALAPKO Workshop, 22. Univ. of Oulu, Dept. of Geoph., Rep., pp. 9–10.

Bahr, K., Simpson, F., 2002. Electrical anisotropy below slow- and fast-moving plates: paleoflow in the upper mantle? Science 295, 1270–1272.

Caldwell, G.T., Bibby, H.M., Brown, C., 2004. The magnetotelluric phase tensor. Geophys. J. Int. 158, 457–469.

Dmitriev, V.I., Berdichevsky, M.N., 1979. The fundamental model of magnetotelluric sounding: a generalized impedance model. IEEE Proc. 67, 1034–1044.

Dmitriev, V.I., Berdichevsky, M.N., 2002. A generalized impedance model. Izvestiya, Phys. Solid Earth 38 (10), 897–903.

Egbert, G.D., 1997. Robust multiple-station MT data processing. Geophys. J. Int. 130, 475–496.

Engels, M., 1997. Untersuchungen zur elektromagnetischen Induktion in Gronland. Dissertation, Goettingen Univ., Cuvillier Verlag, Goettingen, 131 p. (in German).

Engels, M., Korja, T., BEAR WG, 2002. Multisheet modelling of the electrical conductivity structure in the Fennoscandian Shield. Earth Planets Space 54, 559–573.

Ernst, T., Jankowski, J., 2005. On the plane wave approximation of the external geomagnetic field in regional induction studies. Izvestiya, Phys. Solid Earth 41 (5), 363–370.

Feldshtein, Y.I., Levitin, A.E., 1986. Solar wind control of electromagnetic field and currents in the ionosphere. J. Geomagn. Geoelectr. 38, 1143–1182.

Garcia, X., Chave, A.D., Jones, A.G., 1997. Robust processing of MT data from the auroral zone. J. Geomagn. Geoelectr. 48, 1451–1468.

Gordienko, V.V., 2001. Geological criteria and integrated analysis of a zone of recent activity in Fennoscandia. Proceedings of the Institute of Fundamental Studies, pp. 10–15.

Hermance, J.F., 1978. Electromagnetic induction in the Earth by a moving ionospheric current system. Geophys. J. R. Astron. Soc. 55, 557–576.

Jones, A.G., Spratt, J., 2002. A simple method for deriving the uniform field MT responses in auroral zones. Earth Planets Space 54, 443–450.

Jones, A.G., Olafsdottir, B., Tiikkainen, J., 1983. Geomagnetic induction studies in Scandinavia III. MT observations. J. Geophys. 54, 35–50.

Kaikkonen, P., Vanyan, L.L., Hjelt, S.E., Shilovsky, A.P., Pajunpaa, K., Shilovsky, P.P., 1983. A preliminary geoelectric model of the Karelian megablock of the Baltic Shield. Phys. Earth Planet. Inter. 32, 301–305.

Karato, S., 1990. The role of hydrogen in the electrical conductivity of the upper mantle. Nature 347, 272–273.

Korja, T., Hjelt, S.-E., 1993. Electromagnetic studies in Fennoscandian Shield — electrical conductivity of Precambrian crust. Phys. Earth Planet. Inter. 81, 107–138.

Korja, T., Koivukoski, K., 1994. Crustal conductors along the SVEKA profile in the Fennoscandian (Baltic) Shield, Finland. Geophys. J. Int. 116, 173–197.

Korja, T., Smirnov, M.Yu., 2006. Electromagnetic Mini Array (EMMA) project in Finland. Personal communications.

Korja, T., Engels, M., Zhamaletdinov, A.A., Kovtun, A.A., Palshin, N.A., et al., 2002. Crustal conductivity in Fennoscandia — a compilation of a database on crustal conductance in the Fennoscandian Shield. Earth Planets Space 54, 535–558.

Kovtun, A.A., 1989. The structure of the crust and upper mantle in the northwestern East European Platform. LGU, Leningrad. 284 pp. (in Russian).

Kovtun, A.A., Vagin, I.L., Vardanyants, N.P., Legen'kova, N.P., Smirnov, M.Yu., Uspensky, N.I., BEAR WG, 2002. Analysis of magnetotelluric and magnetic variation results in daily variation range from BEAR data and construction of the normal section of the Baltic Shield. Izvestiya, Phys. Solid Earth 38 (11), 935–953.

Kukkonen, I.T., Kinnunen, K.A., Peltonen, P., 2003. Mantle xenoliths and thick lithosphere in the Fennoscandian Shield. Phys. Chem. Earth 28, 349–360.

Lahti, I., Korja, T., Kaikkonen, P., Vaittinen, K., BEAR Working Group, 2005. Decomposition analysis of the BEAR magnetotelluric data: implications for the upper mantle conductivity in the Fennoscandian Shield. Geophys. J. Int. 162, 1–15.

Levitin, A.E., Gromova, L.I., Dremukhina, B.F., Palshin, N.A., 2007. The analysis of the high latitude current systems during the BEAR experiment on the base of IZMEM model. Geomagn. Aeron. 47 (3), 351–356 (in Russian).

Mareschal, M., 1986. Modelling of natural sources of magnetospheric origin in the interpretation of regional induction studies: a review. Surv. Geophys. 8, 261–300.

Olsen, N., 1998. The electrical conductivity of the mantle beneath Europe derived from C-responses from 3 to 720 hr. Geophys. J. Int. 133, 298–308.

Osipova, I.L., Hjelt, S.-E., Vanyan, L.L., 1989. Source field problems in northern parts of the Baltic Shield. Phys. Earth Planet. Inter. 53, 337–342.

Pajunpaa, K., 1987. Conductivity anomalies in the Baltic Shield in Finland. Geophys. J. R. Astron. Soc. 91, 657–666.

Rasmussen, T., Roberts, R., Pedersen, L., 1987. Magnetotellurics along the Fennoscandian long range profile. Geophys. J. R. Astron. Soc. 89, 799–820.

Sandoval, S., Kissling, E., Ansorge, J., SVEKALAPKO Seismic Tomography WG, 2004. High-resolution body wave tomography beneath the SVEKALAPKO array — II. Anomalous upper mantle structure beneath the central Baltic Shield. J. Geophys. Int. 157, 200–214.

Sokolova, E.Yu., Varentsov, I.v.M., EMTESZ WG, 2006. The RRMC technique fights highly coherent EM noise In: Protokoll über das Kolloquium elektromagnetische Tiefenforschung ISSN 0946–7467 21. Kolloquium: Haus Wohldenberg, Holle. 3.-7.10.2005, 124–136.

Schmucker, U., 1999. A spherical harmonic analysis of solar daily variation in the years 1964–1965: response estimates and source fields for global induction. I. Methods, II. Results. J. Geophys. Int. 136 (2), 439–476.

Schmucker, U., 2003. Horizontal special gradient sounding and geomagnetic depth sounding in the period range of daily variation. In: Protokoll über das Kolloquium elektromagnetische Tiefenforschung ISSN 0946 - 7467 20. Kolloquium: Konigstein. 29.09 - 3.10. 2003, 228–237.

Semenov, V.Yu., 1998. Regional conductivity structures of the Earth's mantle. Publ. Inst. Geophys., Pol. Acad. Sci. C-65 (302) (122 pp.).

Smirnov, M.Yu., 2003. Magnetotelluric data processing with a robust statistical procedure having a high breakdown point. Geophys. J. Int. 152, 1–7.

Viljanen, A., Pirjola, R., Amm, O., 1999. Magnetotelluric source effect due to 3D ionosperic current systems using the complex image method for 1D conductivity structures. Earth Planets Space 51, 933–945.

Vanyan, L.L., Palshin, N.A., Levitin, A.E., BEAR WG, 2002a. Two types of the ionospheric source in high latitudes. XVI Workshop on EM Induction in the Earth (Abstracts). Santa Fe, USA. EM4.11.

Vanyan, L.L., Kuznetsov, V.A., Lyubetskaya, T.V., Palshin, N.A., Korja, T., BEAR WG, 2002b. Electrical conductivity of the crust beneath Central Lapland. Izvestiya, Phys. Solid Earth 38 (10), 798–815.

Varentsov, Iv.M., 2002. A general approach to the magnetotelluric data inversion in a piecewise-continuous medium. Izvestya, Phys. Solid Earth 38 (11), 913–934.

Varentsov, Iv.M., Engels, M., Korja, T., Smirnov, M.Yu., BEAR WG, 2002. A generalized geoelectric model of Fennoscandia: a challenging database for long-period 3D modeling studies within the Baltic Electromagnetic Array Research (BEAR) project. Izvestya, Phys. Solid Earth 38 (10), 855–896.

Varentsov, Iv.M., Sokolova, E.Yu, Martanus, E.R., Nalivaiko, K.V., BEAR WG, 2003a. System of EM field transfer operators for the BEAR array of simultaneous soundings: methods and results. Izvestya, Phys. Solid Earth 39 (2), 118–148.

Varentsov, Iv.M., Sokolova, E.Yu, BEAR WG, 2003b. Diagnostics and suppression of auroral distortions in the transfer operators of the EM field in the BEAR experiment. Izvestya, Phys. Solid Earth 39 (4), 283–307.

Weidelt, P., 1978. Entwicklung und erprobung eines verfahren zur inversion zweidimensionaler leitfahigkeitsstrukturen in E-polarisation. Dissertation, Gettingen Univ. (in German).

Wessel, P., Smith, W.H.F., 1998. New, Improved Version of Generic Mapping Tools Released. Eos, Trans. – Am. Geophys. Union 79 (47), 579.